



UNIVERSITY OF LEEDS

This is a repository copy of *Variations from dry to aquatic conditions in Vertisols (Esplugafreda Formation, Eastern Pyrenees, Spain): Implications for late Paleocene climate change.*

White Rose Research Online URL for this paper:

<https://eprints.whiterose.ac.uk/186029/>

Version: Accepted Version

Article:

Basilici, G, Colombera, L orcid.org/0000-0001-9116-1800, Soares, MVT et al. (6 more authors) (2022) Variations from dry to aquatic conditions in Vertisols (Esplugafreda Formation, Eastern Pyrenees, Spain): Implications for late Paleocene climate change. *Palaeogeography, Palaeoclimatology, Palaeoecology*, 595. 110972. p. 110972. ISSN 0031-0182

<https://doi.org/10.1016/j.palaeo.2022.110972>

© 2022 Elsevier B.V. All rights reserved. This manuscript version is made available under the CC-BY-NC-ND 4.0 license <http://creativecommons.org/licenses/by-nc-nd/4.0/>

Reuse

This article is distributed under the terms of the Creative Commons Attribution-NonCommercial-NoDerivs (CC BY-NC-ND) licence. This licence only allows you to download this work and share it with others as long as you credit the authors, but you can't change the article in any way or use it commercially. More information and the full terms of the licence here: <https://creativecommons.org/licenses/>

Takedown

If you consider content in White Rose Research Online to be in breach of UK law, please notify us by emailing eprints@whiterose.ac.uk including the URL of the record and the reason for the withdrawal request.



eprints@whiterose.ac.uk
<https://eprints.whiterose.ac.uk/>

Variations from dry to aquatic conditions in Vertisols (Esplugafreda Formation, Eastern Pyrenees, Spain): Implications for late Paleocene climate change

Giorgio Basilici^{a,b}, Luca Colombera^c, Marcus Vinícius Theodoro Soares^a, Oscar Javier Arévalo^c, Nigel Philip Mountney^c, Paolo Lorenzoni^d, Carlos Roberto de Souza Filho^a, Áquila Ferreira Mesquita^a, Juraj Janočko^e

a) Department of Geology and Natural Resources, Institute of Geosciences, State University of Campinas, 13083-870 Campinas, SP, Brazil

b) Centro Regional de Investigaciones Científicas y Transferencia Tecnológica, La Rioja / CONICET, Argentina

c) Fluvial, Eolian & Shallow-Marine Research Group, School of Earth and Environment, University of Leeds, Leeds LS2 9JT, UK

d) Professional consultant, Largo Trasimeno 1, 02100 Rieti, Italy

e) Institute of Geosciences, Faculty BERG, Technical University of Kosice, Letna 9, 040 11 Košice, Slovakia

Abstract

Sedimentological studies of ancient fluvial systems commonly do not consider in detail palaeosols in floodplain deposits. This is the case of the upper Paleocene Esplugafreda Formation (Pyrenees, Spain), a 100–340 m thick alluvial succession, in which palaeosols represent more than 80% of its thickness. This unit closely predates the climate crisis of the Paleocene/Eocene transition, the PETM (Paleocene/Eocene Thermal Maximum). The purpose of this paper is to define the palaeoenvironmental conditions of formation of these palaeopedogenic conditions, and to establish possible changes during the late Paleocene directly prior to the onset of the PETM. This paper analyses the palaeosols in terms of variations in ‘aquic conditions’, concerning to water saturation, reduction and formation of redoximorphic features in soils. The uppermost part of the Esplugafreda Formation consists of cumulative sandy mudstone palaeosols, laterally associated with sparse channel deposits. Two pedotypes were recognised: Pont d'Orrit and Areny. A mud content >60% (mainly montmorillonite), pedogenic slickensides, wedge-shaped aggregates, mukgara and blow structures indicate that both pedotypes belong to the Vertisol order. They reveal a climate characterised by strong seasonal moisture variations. The Pont d'Orrit pedotype, which dominates the lower portion of the succession, shows reddish brown horizons (Bss), calcareous nodules concentration (Bssk horizon) and scarce redoximorphic features, which indicate a semi-arid climate. The Areny pedotype, which prevails in the upper part, shows a yellow horizon (Bssg) containing goethite and abundant redoximorphic features, which reveal aquatic conditions. There is no clear sedimentological evidence that river flooding became relatively more frequent in the upper part of the succession, suggesting that the aquatic conditions were caused by an increase in precipitation. This study demonstrates that (i) changes in some pedogenic features within the Vertisols enable interpretation of palaeoenvironmental variations and (ii) this region experienced a changing climate in the late Paleocene, before the onset of the PETM.

Keywords

Cumulative palaeosol
Surface-water gley
Floodplain succession
Trempe-Graus Basin
Alluvial deposits

1. Introduction

Relatively few studies of fluvial successions have examined floodplain deposits in detail from the physical sedimentological and palaeopedological perspective (e.g.: Kraus and Aslan, 1993; McCarthy et al., 1997; Joeckel et al., 2017; Milroy et al., 2019). In part, this may reflect the fact that floodplain deposits are commonly composed of palaeosols. De facto, the analytical approach to the study of palaeosols is distinctly different from the methods applied to sedimentary rocks that did not undergo any significant post-depositional pedogenesis, and this may dissuade sedimentologists from considering these deposits. Nevertheless, two considerations should encourage sedimentologists who examine continental successions to integrate palaeosols analyses in their studies: (i) many fluvial sedimentary successions consist of palaeosols from 55 to 95% of their thickness (Bown and Kraus, 1987; Kraus and Aslan, 1993; McCarthy et al., 1997; Basilici, 2000; Basilici and Dal' Bo, 2010, Basilici et al., 2016, Basilici et al., 2017; Joeckel et al., 2017; Soares et al., 2020), and (ii) palaeosols hold information on the palaeoenvironmental conditions that cannot be recorded in sediments, since their genesis depends on variables that may not influence sedimentary processes and because they act as open systems for a long time (potentially over hundreds to millions of years in some cases) (Jenny, 1941; Duchaufour, 1982; Retallack, 2001).

Since the 1980s, several papers have reported on the relationships between palaeosols and depositional processes in alluvial systems (e.g.: Bown and Kraus, 1987; Kraus and Aslan, 1993; Marriott and Wright, 1993; McCarthy et al., 1997; Basilici and Dal' Bo, 2010; Basilici et al., 2016; Basilici et al., 2017; McCarthy and Plint, 2017; Joeckel et al., 2017; Soares et al., 2020); notwithstanding, they only represent a small fraction of the published literature on alluvial depositional palaeoenvironments. This is mirrored in the literature on the Esplugafreda Formation (Paleocene, Pyrenees, Spain; Fig. 1), in which very detailed studies on channelised or non-channelised alluvial deposits have already been published (Dreyer, 1993; Pujalte et al., 2014; Colombera et al., 2017; Arévalo et al., 2022), but in which no detailed account of its fine-grained pedogenically-altered floodplain deposits exists, in spite of them representing more than 80% of this unit.

The Esplugafreda Formation was deposited in an alluvial setting, probably associated with different coalescing fans arising from the Pyrenean mountain front (Dreyer, 1993). This unit is overlain by the Claret Formation, which is also continental in origin, and whose second member was recognised as bearing a record of the global climate crisis of the Paleocene-Eocene Thermal Maximum (PETM) (Schmitz and Pujalte, 2003, Schmitz and Pujalte, 2007). This climate event caused a global rise of temperature of 5–9 °C or higher, as well as a reorganisation of the global hydrological cycle, which in the study area is thought to have led to an increase in precipitation (Kennett and Stott, 1991a, Kennett and Stott, 1991b; Zachos et al., 2006; Pagani et al., 2006; Schmitz and Pujalte, 2007; McInerney and Wing, 2011; Charles et al., 2011; van Dijk, 2019; Shields et al., 2021; Rush et al., 2021). However, evidence of fluvial reorganisation, which consists of an increase in the number, dimension and lateral interconnection of the channel bodies (c.f., building block C6 of Dreyer, 1993) and which may be associated with climatic causes (Dawson et al., 2014), has been recognised in portions of the stratigraphy that predate the onset of the PETM: the uppermost portion of the Esplugafreda Formation (Dreyer, 1993) and the lowermost member of the Claret Formation (Pujalte et al., 2014; Colombera et al., 2017; Arévalo et al., 2022).

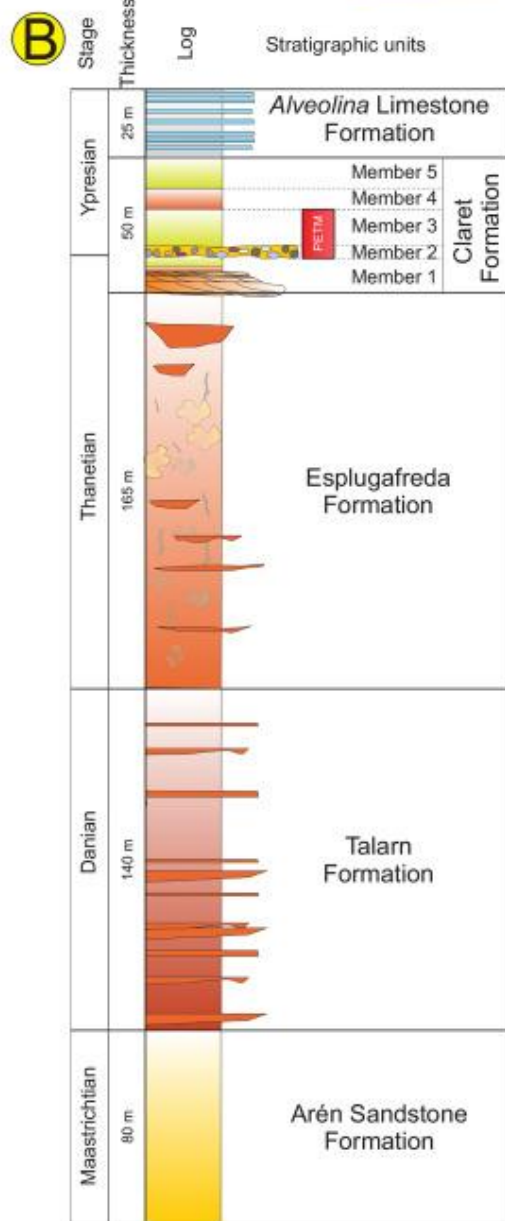
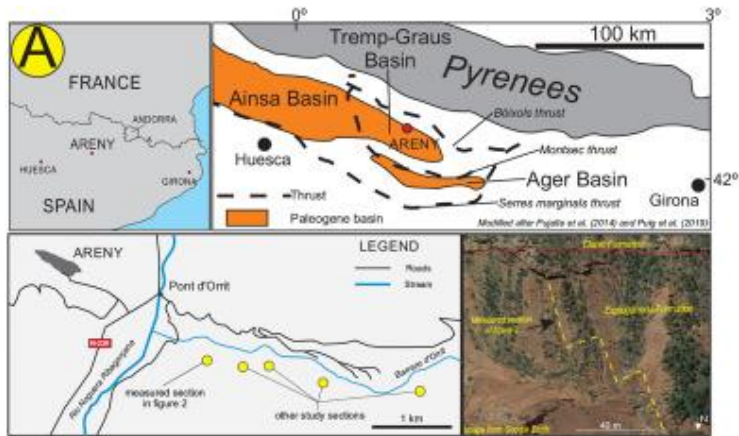


Fig. 1. (A) Geographic location and geological setting of the study area. (B) General stratigraphic section of the study area. Note the stratigraphic position of the PETM (Paleocene-Eocene Thermal Maximum) in the Claret Formation. Data and figure modified from Cuevas (1992), Pujalte and Schmitz (2005), Institut Geològic de Catalunya (2010) and Pujalte et al. (2014) and Puig et al. (2019). Orbital image from Google Earth©.

The aim of this paper is to show how palaeosols are a useful tool for inferring the palaeoenvironmental conditions in sedimentary successions of floodplain origin. Specific objectives of this paper are as follows: (i) to examine possible palaeoenvironmental variations in the floodplain succession of the Esplugafreda Formation and (ii) to verify whether the Esplugafreda Formation records palaeoenvironmental change that may have heralded the PETM, as hypothesised by Dawson et al. (2014).

2. Location and geological context

2.1. The Esplugafreda Formation

The study succession corresponds to the uppermost portion of the Esplugafreda Formation, a Paleocene unit that is particularly well exposed along the narrow valley, the Barranc d'Orrit, N125 from the town of Areny (Aragon, Spain) (Fig. 1A). This unit lies in the Tremp-Graus Basin, which contains deposits of continental, paralic and marine origin, displaying a deepening trend towards the basin axis and its western part. The Tremp-Graus Basin (Fig. 1A) is a thrust-sheet top basin (Allen and Allen, 2005), formed as consequence of the Cretaceous to Early Miocene collision of the Iberian and European plates. It developed on the back of the Montsec thrust sheet and south of the Bóixols thrust (Puigdefàbregas and Souquet, 1986; Puigdefàbregas et al., 1992; Vergés et al., 1995; Vergés and Burbank, 1996; Puig et al. (2019)). The dynamics of these thrusts have generated a basin morphology characterised by steep northern margins and gentler southern ones. The basin shows a NNW axis, parallel to the orogen, with a general drainage direction to the west (Vergés and Burbank, 1996; Whitchurch et al., 2011). The sedimentary succession that filled this basin, originally named "Garumnian facies", was defined by Cuevas (1992) as the Tremp Group, the stratigraphy of which was partially redefined by Pujalte and Schmitz (2005). Physical stratigraphic correlations, biostratigraphy and chemostratigraphy allow the age of this unit to be determined as Maastrichtian to Ypresian (Schmitz and Pujalte, 2003; Pujalte and Schmitz, 2005). It contains continental deposits that interfinger to the west with marine limestone. In the study area the following units are recognised from the bottom to the top: Arén Sandstone, Talarn, Esplugafreda, Claret and Alveolina limestone formations (Fig. 1B). The Esplugafreda Formation consists of various types of channelised and non-channelised pebbly sandstone strata encased in pedogenically-altered reddish brown floodplain sandy mudstones (>80% of the thickness), which were probably deposited in a relatively distal portion of an alluvial system (see details in: Cuevas, 1992; Dreyer, 1993; Pujalte et al., 2014; Colombera et al., 2017; Arévalo et al., 2022). The thickness of this unit varies from 100 to 340 m (Dreyer, 1993; Schmitz and Pujalte, 2007; Institut Geològic de Catalunya, 2010); in the study area its thickness is 165 m (Baceta et al., 2011). The Claret Formation, 10–70 m thick, overlies the Esplugafreda Formation; the contact is marked by an erosional surface that defines the base of a system of palaeovalleys (Pujalte et al., 2014). The Claret Formation is formed by sandy-conglomerate channel bodies interlayered with pedogenically-altered sandy mudstone, and it is divided by Pujalte and Schmitz (2005) into five informal members. This formation is conformably overlain by marine limestone and marl (Alveolina Limestone Formation). Between the second and the fourth member of the Claret Formation, Schmitz and Pujalte, 2003, Schmitz and Pujalte, 2007 recognised the stratigraphic record of the Paleocene-Eocene Thermal Maximum (Fig. 1B) based on identification of the characteristic carbon isotope excursion.

2.2. The Paleocene-Eocene thermal Maximum (PETM)

The PETM, which is globally identified by a negative carbon isotope excursion (CIE), was characterised by a sharp increase in global temperature (5° to 9° in 10 ky), which occurred across the

Paleocene-Eocene boundary (55.8 Ma ago), and which was followed by a slow decline to previous temperatures that took between 100 and 200 ky (Kennett and Stott, 1991a, Kennett and Stott, 1991b; Zachos et al., 2006; Pagani et al., 2006; McInerney and Wing, 2011; Charles et al., 2011; van Dijk et al., 2020). The effects of this global warming, which triggered an enhanced hydrological cycle, seem to have differed across the globe with an increase in rainfall at high latitudes and more arid conditions at low latitudes (Kender et al., 2012; Carmichael et al., 2017). However, the effect of the PETM global warming in alluvial systems seems to have varied geographically. For example, in relation to the Claret Formation (Catalan Pyrenees), Schmitz and Pujalte (2007), Colomera et al. (2017) and Chen et al. (2018) asserted that the PETM crisis modified the hydrological cycles in a way that significantly altered the geometry and mobility of the alluvial channel network. In the Salta Basin (NW, Argentina), Andrews et al. (2017) used carbon isotope data to pinpoint the PETM interval in a palaeosol succession and applied to the local interval of PETM geochemical climofunctions. They recognised changes in mean annual temperature and palaeoprecipitation from pre-PETM to PETM interval: from 5 to 10 °C to 11–16 °C (Andrews et al., 2017; their Fig. 12) and from 1000 mm/y to 1500 mm/y (Andrews et al., 2017; their Fig. 10), respectively. Conversely, for the Willwood Formation of the Bighorn Basin (Wyoming, USA), which was located at the same palaeolatitude, Kraus et al. (2015) inferred that the PETM caused a reduction of precipitation with consequent storing of the sediments in upstream areas, thereby decreasing the rate of sediment transfer to the alluvial basin.

Some authors recognised climatic variations in sedimentary successions that precede the CIE. Dawson et al. (2014) hypothesised, but could not prove with evidence, that the olive yellow horizons of the uppermost portion of the Esplugafreda Formation may testify to an increase of precipitation. In this perspective, it should be noted that Sluijs et al. (2007), based on palaeontological (dinoflagellate cysts) and geochemical data from cores of the New Jersey continental shelf, recognised a warming trend whose onset preceded the CIE by some thousands of years. Similarly, Kender et al. (2012), based on palynological, dinoflagellate cysts, geochemical and sedimentological proxies from a North Sea core, inferred an enhanced hydrological cycle, which caused an increase in precipitation, river discharge and terrigenous input, which started before the time corresponding to the base of the CIE.

3. Materials and methods

The data considered in this paper are based on field macroscopic observations, micromorphological analyses of thin sections, and mineralogical and organic carbon analyses of samples of palaeosols and related deposits. A stratigraphic section of c. 90 m in the upper portion of the Esplugafreda Formation was measured at centimetre-scale resolution (Fig. 2). Three other sections, along the Barranc d'Orrit (Fig. 1), with a cumulative total thickness of 95 m, were logged at the same level of detail; the sections are distributed along a 3.2 km long W-E transect. These latter three sections are not presented in detail in this study, but these complementary data were considered in the description of the palaeosol profiles.

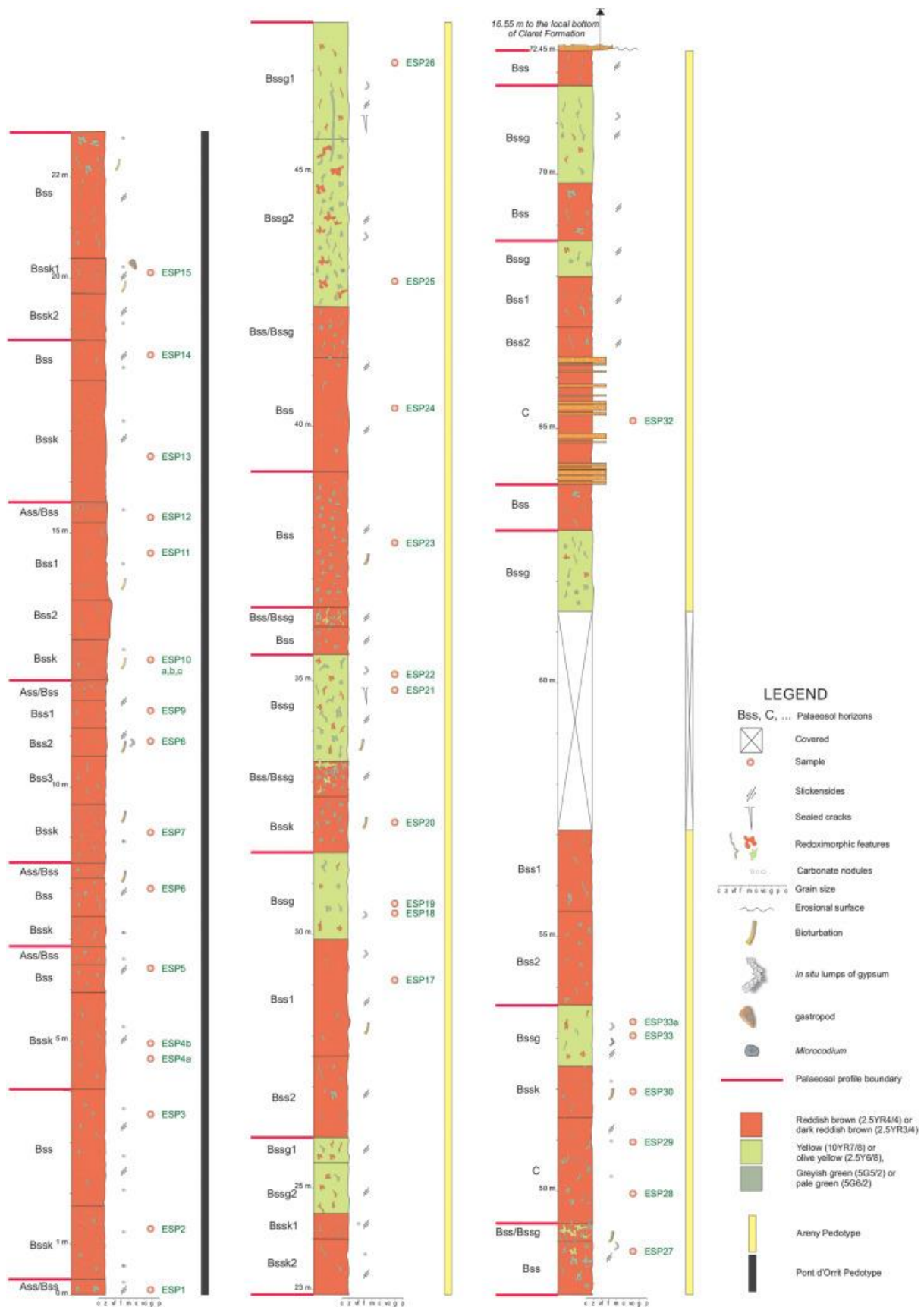


Fig. 2. Detailed stratigraphic section of the uppermost portion of the Esplugafreda Formation. The section was measured along the Barranc d'Orrit, geographical coordinates (42°14'52"N–0°44'33"W). The 16.15 m of stratigraphy directly underlying the Claret Formation is here constituted of c.11 m of channelised sandstones and 5 m of Bssg and Bss horizons of sandy mudstones. See Fig. 1A to localise the stratigraphic section.

In the field, palaeosols and deposits were macroscopically described. Recognition of the palaeosol profiles and horizons were made following the Soil Science Division Staff (2017). The palaeosols were described according to macroscopic and microscopic (micromorphological) aspects. Macroscopic descriptions encompassed thickness, horizon boundaries, texture, colour, structures, redoximorphic features, fossils and ichnological features, following the field guide of Schoeneberger et al. (2012). Colour was defined in fresh sample under sunlight conditions according to the Munsell colour scale (Munsell Color, 2013). Charts for estimating abundance were applied to determine proportions of colours, calcareous nodules and redoximorphic features based on field observations and of grain-size classes, Microcodium fragments and micromass in thin sections. The deposits interlayered with the palaeosols, which constitute less than 7% of the thickness of the measured section (Fig. 2), were described according to their bedding geometry and sedimentary structures. Microscopic optical analyses in thin sections were useful to define their textural and microstructural features.

More than 70 samples were collected in steep exposures from the middle of each horizon after 0.2 m deep excavation, to expose pristine material unaltered by current pedogenesis. Thirty-five thin sections were obtained by impregnation with epoxy resin, to allow micromorphological description according to Bullock et al. (1985) and Stoops (2003). Grain size is defined according to microscopic analyses referring to the Wentworth's Scale (Wentworth, 1922). The mineral composition of 25 samples, including both the pedotypes described (see below), was established based on visible-infrared (400–2500 nm) reflectance spectroscopy (Clark, 1999), using an Analytical Spectral Devices (ASD) spectrometer (FieldSpec-4). This is an optimal, non-destructive method for determination of iron oxides (haematite), hydroxides (goethite), multiple clays, micas and carbonates (e.g., Asadzadeh and Souza Filho, 2016). Quantitative analyses of total organic carbon (TOC) were carried out in 28 triplicate samples of the palaeosol horizons. The samples were comminuted into particles that are less than 75 µm in diameter and were then treated with 10% (v/v) HCl to eliminate inorganic carbon. The TOC content was obtained by combustion at 1150 °C using a TOC analyser equipped with a Solids Module (HT 1300 - Multi N/C 2100, Analytik Jena) at the Laboratory of Geochemistry of Institute of Geosciences (University of Campinas, Brazil). Analysis of vertical transition statistic, based on the Markov chain, was undertaken to establish the trend of vertical juxtaposition of the palaeosol horizons (see Supplementary Material 1).

The palaeosol profiles were distinguished in pedotypes. A pedotype is defined as “simply a kind of soil or palaeosol as recognized in the field” (Retallack, 1994, p.1337). The classification of the palaeosols followed the criteria by Soil Survey Staff, 1999, Soil Survey Staff, 2014. This classification has been applied based on the original characteristics that can still be recognised in the palaeosols. The interpretation of the micromorphological features is based on Stoops et al. (2010).

To facilitate the comprehension of this article by a broad readership, a synthetic glossary of the pedological and palaeopedological terms used in the text is provided (see Supplementary Material 2).

4. Palaeosol profiles and pedotypes

The sedimentary succession consists of sandy mudstone that transitions laterally to thin tabular- and ribbon-like bodies of fine- and medium-grained sandstone and sandy conglomerate. More than 90% of the thickness of the measured succession is formed of palaeosol profiles; the remainder of the succession is composed of non-channelised sandstone and sandy mudstone deposits that appear only in the upper portion of the stratigraphic section (Fig. 2). This section focuses on the description

of the palaeosols. Fine- grained non-channelised deposits have been described as part of the C horizon; medium- to very fine-grained sandstone deposits are not described because they are not the subject of this study. See Dreyer (1993), Colomera et al. (2017) and Arévalo et al. (2022) for detailed descriptions of the sandstone and conglomerate deposits. Two pedotypes were recognised in the study succession, which have been termed as Pont D'Orrit and Areny pedotypes (Fig. 3).

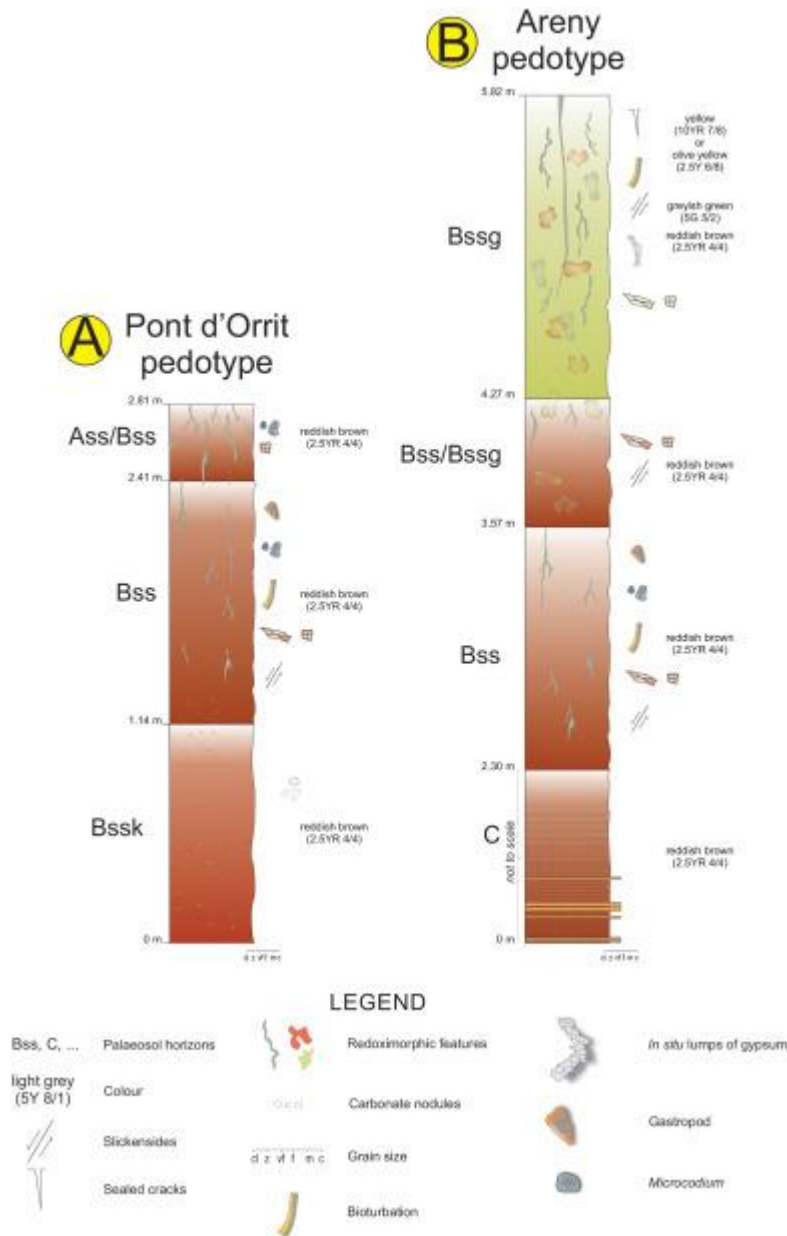


Fig. 3. Graphical synthesis of the pedotypes. The thickness of the horizons is based on the mean value of all the measurements.

4.1. Pont d'Orrit pedotype

This pedotype constitutes the totality of the lower portion of the study succession (Fig. 2). Its thickness varies from 1.65 to 4.1 m, with a mean of 3.2 m, and its profile consists of the following horizons, indicated with respective percentages of the total thickness: Ass/Bss (9%) - Bss (50%) - Bssk (41%). The horizons are characterised as follows.

4.1.1. Ass/Bss horizon

Ass/Bss is a reddish brown (2.5YR 4/4) or red (2.5YR 4/6) sandy mudstone horizon (Fig. 3A). This horizon is 0.35–0.40 m thick. Its upper adjacent horizon is Bssk and the lower is Bss; the vertical transitions have a diffuse distinctness and a smooth topography (Fig. 4A). The coarse fraction (>62 μm) of the groundmass is formed of sparitic calcite clasts (0.05–0.1 mm) attributable to fragments of *Microcodium*; their frequency distribution is c. 20% of microscope area (Fig. 4B). *Microcodium* occurs also in locally abundant aggregate forms, which are constituted of fibrous-radiating sparitic calcite crystals, 0.4 mm wide and 1–2 mm long, showing a typical *épis de maïs* and rosette (sensu Lucas and Montenat, 1967) or corn-cob and rosette forms (sensu Kabanov et al., 2008) (Fig. 4C). The micromass (<62 μm) is mainly formed of expandable clays (montmorillonite) impregnated with of Fe/Mn oxides (see below). The c/f (coarse/fine) related distribution pattern is open to single spaced porphyric. The micromass is characterised by stipple- or mosaic-speckled b-fabric (birefringence fabric) (Fig. 4B).

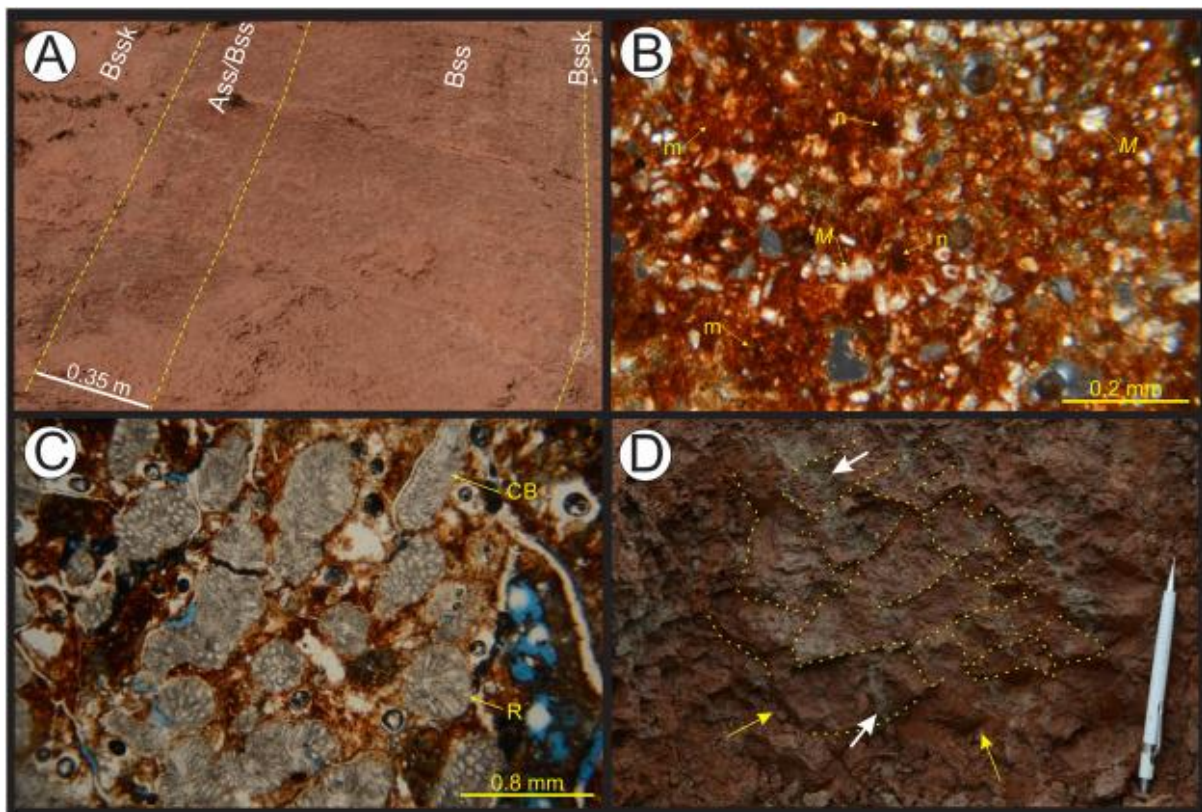


Fig. 4. Pont d'Orrit pedotype. (A) The Ass/Bss horizon is distinguished on the increase of the tubular redoximorphic features interpreted as rhizohaloes (Kraus and Hasiotis, 2006). (B) Photomicrograph of the Ass/Bss horizon. The coarse fraction of the groundmass is formed by disaggregated fragments of *Microcodium* (white colour clasts, M). Impregnative redox features are visible: nodules (n) and masses (m). The grey "mottles" are holes. The c/f related distribution pattern is porphyric and b-fabric is stipple- or mosaic-speckled. XPL. (C) Ass/Bss horizon. Aggregate forms of *Microcodium*, in corn-cob (CB) or rosette (R) appearance (Kabanov et al., 2008). PPL. (D) Ass/Bss horizon. Tubular redox depletion features are interpreted as rhizohaloes (white arrow). Slickenside surfaces (yellow arrow) divide angular blocky peds, the boundaries of which are indicated by stippled yellow lines. Clutch pencil: 142 mm.

Macroscopic redox depletion features are abundant in this horizon: their distribution varies from 20 to over 40% (mean 25%) of the exposed surface. They consist of greyish green (5G 5/2) elongated and irregular forms, approximately perpendicular to the bedding surface, locally more than 0.3 m long, with circular sections of 10–40 mm in diameter and at places branching downwards (Fig. 4A and D). Some redox depletions are amiboidal in shape and are developed on smooth surfaces. These surfaces, attributable to pedogenic slickensides, have dimensions up to 50 × 50 mm², display thin and parallel grooves and divide coarse angular blocky peds (40–50 mm in diameter) (Fig. 4D). In thin section, redoximorphic amorphous Fe/Mn concentrations of nodules and mass occur (Fig. 4B and C).

4.1.2. Bss horizon

This horizon is reddish brown (2.5YR 4/4) or red (2.5YR 4/6) and it is constituted of poorly sorted, very fine-grained sandy mudstone. The thickness varies from 0.5 to 2.7 m, and is on average 1.27 m (Fig. 3A). The transition to the Ass/Bss horizon is marked by an increase of greyish green (5G 5/2) redox depletion features; the transition to Bssk horizon is characterised by an increase of calcareous nodules and decrease in redox depletions. The lower and upper boundaries of this horizon exhibit diffuse distinctness (0.15 to 0.4 m) and smooth or occasionally wavy topography (Fig. 4 E and F). The coarse fraction (>62 μm) consists of small (0.07–0.15 mm in diameter), angular or subangular, disaggregated fragments of *Microcodium*, embedded in a dense groundmass. Their abundance varies from 5 to 40%, more commonly 20–30% (Fig. 6A). Angular, monocrystalline quartz grains, 0.06 to 0.3 mm in diameter, with undulose extinction are very rare (≤1% in abundance). The micromass is c. 60–80% in abundance and mainly composed of expandable clay montmorillonite (see below). The micromass is impregnated with an amorphous concentration of Fe/Mn oxides, which gives it a reddish brown or red colour; where this impregnation is lacking the micromass shows a stipple-speckled or less commonly mosaic-speckled b-fabric (Fig. 6B). The more common c/f related distribution pattern is single spaced porphyric, but a close to open porphyric occurs locally (Fig. 6A). Rare planar voids separating micropeds can be observed (Fig. 6C).

Small tortuous or spot aggregates of fibrous-radiate crystals of sparitic calcite up to 0.1 m long, attributable to *Microcodium* (Kabanov et al., 2008), cover locally an area around 20% of the exposure in some horizons of this type (Fig. 6D). In thin section, they display corn-cob and rosette forms, 0.4–0.5 mm wide and developed along lines, several millimetres long (Fig. 6E).

Smooth surfaces, less than 10 × 10 mm² to 60 × 60 mm², showing striations and grooves are very common (Fig. 6F). These, which are identified as slickensides, separate medium (less than 50 mm in diameter) to very fine (less than 10 mm in diameter) wedge-shaped peds (Fig. 6G) or coarse (20–30 mm in diameter) to medium (10–20 mm in diameter) angular blocky peds (Fig. 6H). In thin sections, the pedality grade is moderately developed: ultrafine to very fine (0.6–1.5 mm in diameter), subangular blocky micropeds with accommodated faces are observed (Fig. 6C).

Macroscopic redox depletion features (mottles) show a distribution on the exposure surface between 5 and 10%. They consist in four types: (i) large cylindrical forms; (ii) small cylindrical forms; (iii) irregular masses on the glossy surfaces (slickensides); (iv) other features. All the types are greyish green (5G 5/2), they have sharp boundaries with the matrix colour, generating a prominent contrast. Details of each type are as follows. (i) The large cylindrical forms are tortuous or rectilinear, approximately perpendicular to the bedding surface and branching downward. Their transverse section is circular, with diameter of 5–40 mm; they are typically 0.05–0.3 m long, but in the best exposures it is possible to see that are some more than 2 m long (Figs. 5B and 7A). Rarely horizontal

cylindrical forms, up to 0.5 m long and 25 mm in diameter, are observed (Fig. 7B). Locally, these forms show a weak red (10R5/3 or 5/4) nucleus (Fig. 7A and B). (ii) Small cylindrical forms are similar to the larger forms, but <20 mm long and ≤ 1 mm in diameter (Fig. 7C). These forms are also visible in thin section (Fig. 6A). (iii) On the smooth surfaces, greyish green amiboidal areas (mottles), typically with size of 10×10 mm², occur (Fig. 6H). (iv) Other greyish green redox depletions can be found around the aggregates of *Microcodium* and bioturbation tubes. In thin section they appear as depletion hypo-coating pedofeatures.

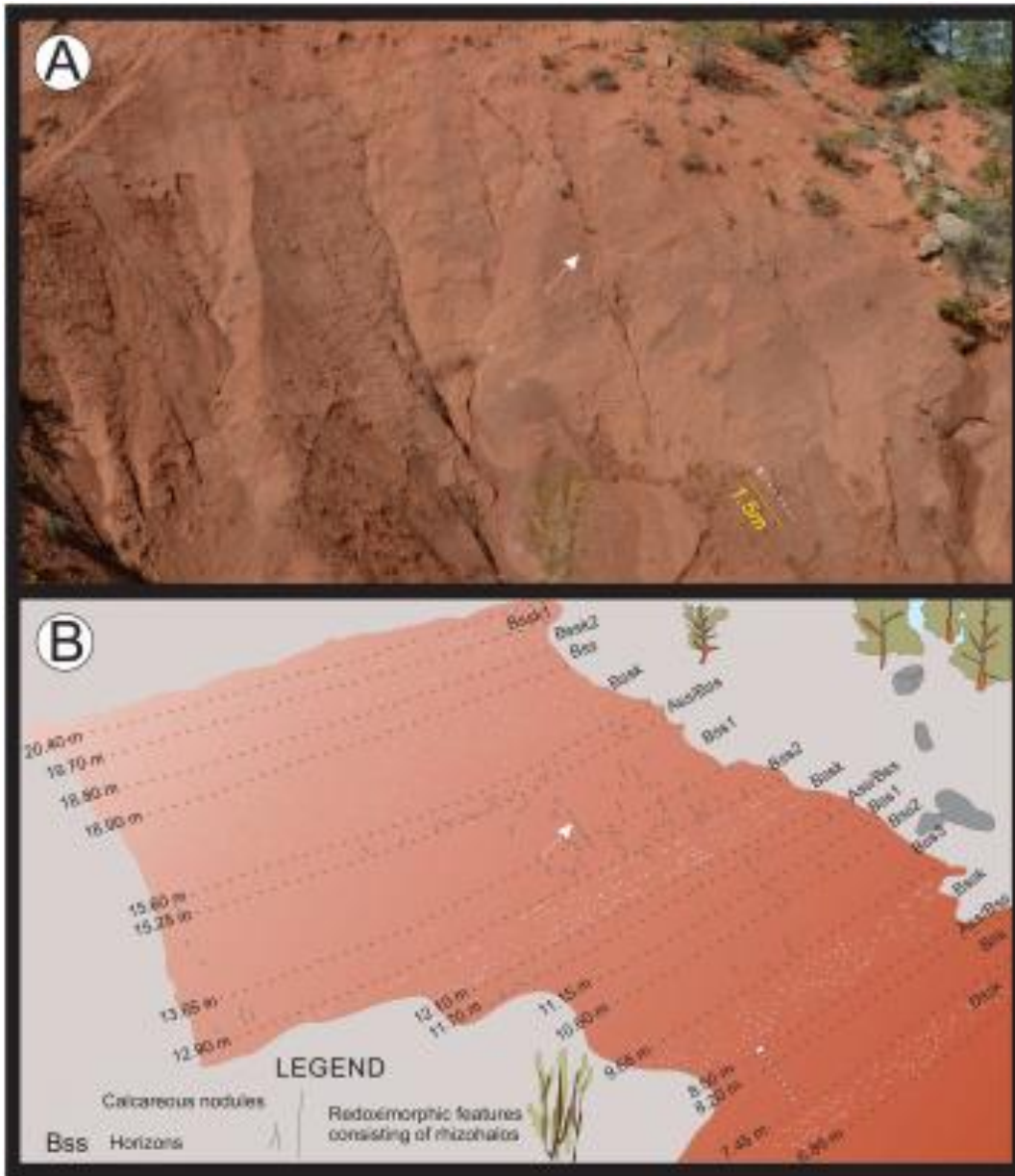


Fig. 5. Pont d'Orrit pedotype. (A) and (B) Photograph and graphical sketch of the lower portion of the study succession, which is characterised by the Pont d'Orrit pedotype. A diffuse transition between all the horizons can be observed. The white arrow shows a long (c. 1.2 m long) redox depletion attributable to rhizohalo. The stratigraphic levels correspond to those in Fig. 2.

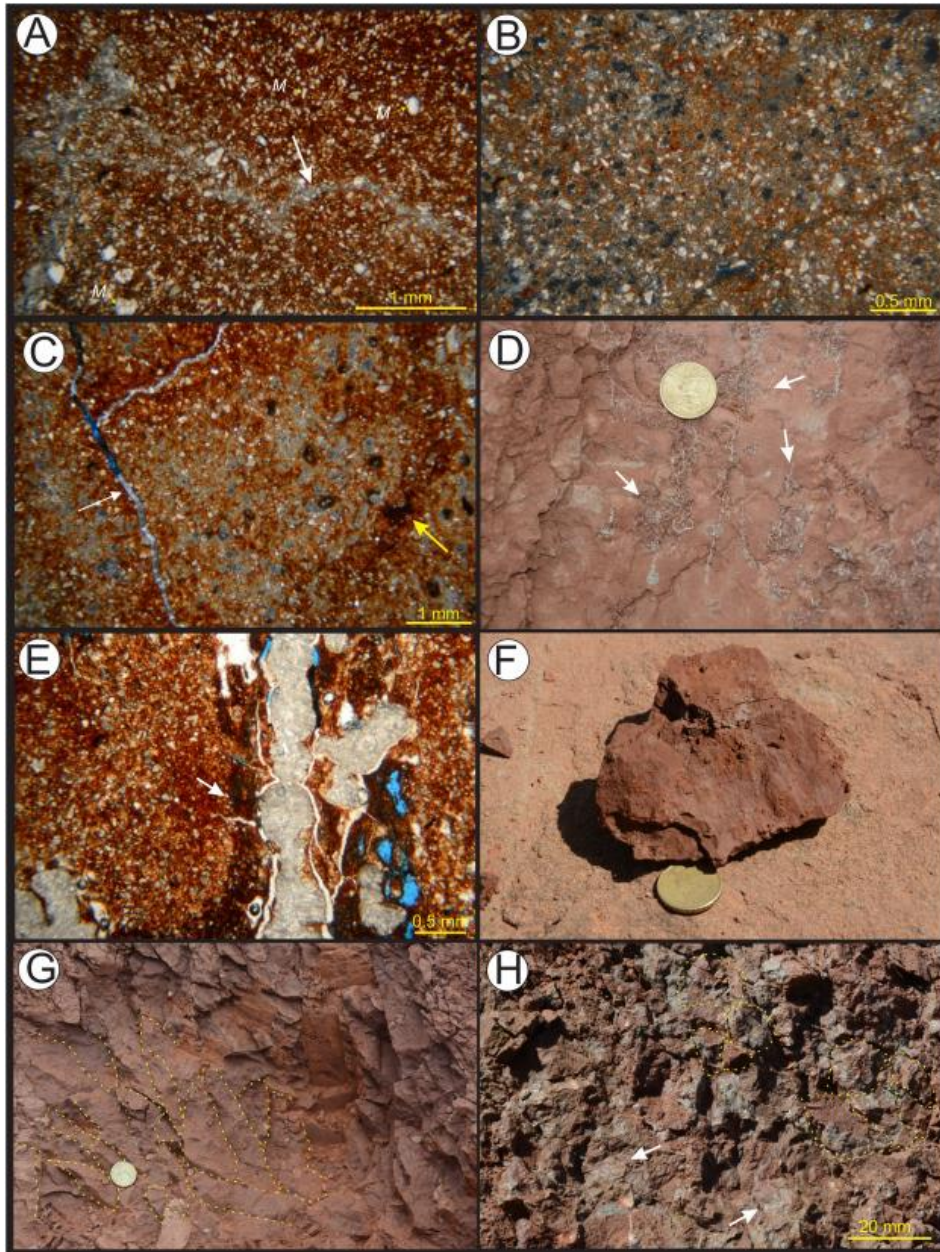


Fig. 6. Pont d'Orrit pedotype. (A) Photomicrograph of Bss horizon showing single spaced porphyric c/f related distribution pattern. Coarse fraction is constituted of Microcodium fragments and the micromass is impregnated of an original (i.e., typical of the parent material) amorphous concentration of Fe/Mn oxides. Note (white arrows) the cylindrical redox depletion attributable to rhizohalo. PPL. (B) Bss horizon. Where the amorphous covering of Fe/Mn oxides are lacking stipple-speckled or mosaic-speckled b-fabric (birefringence fabric) characterise the micromass. The grey "mottles" are holes. XPL. (C) Photomicrograph of subangular blocky microped with probable impregnative Fe/Mn oxide internal hypo-coating. On the left (white arrow) planar voids separating the microped can be seen. On the right the yellow arrow indicates the border of the microped. XPL. (D) Aggregates of Microcodium in life-position (white arrows) are very abundant in the Pont d'Orrit pedotype. Coin: c. 20 mm. (E) Aggregates of Microcodium in thin section in a typical corn-cob form. Note the impregnative redox of Fe/Mn around the specimens (white arrow). PPL. (F) Grooved slickensides surfaces. These surfaces separate wedge-shaped peds showed in Fig. 6F. Coin: c. 20 mm. (G) Wedge-shaped peds separated by slickensides surfaces. These structures are typical of Vertisols. Dashed yellow lines point out the boundaries of the wedge-shaped peds. Coin: c. 20 mm. (H) Coarse to medium angular blocky peds separated by slickensides (see white arrows). Some peds are highlighted by dashed yellow lines. Note the greyish green (5G5/2) redox depletions on the slickenside surfaces.

Large and small cylindrical forms are rhizohaloes (Kraus and Hasiotis, 2006) or drab haloed root traces (Retallack, 2001), which correspond to Fe/Mn depleted areas around a root hole. Stagnant water and organic material of the rotting root create anoxic conditions that deplete the groundmass of Fe/Mn around the root hole generating the greyish green colour (Vepraskas, 2015). Similar conditions caused the irregular greyish green “mottles” on the glossy surfaces (slickensides) and around aggregates of *Microcodium* and bioturbation tubes, probably associated with small roots on the surface of slickensides and organic matter linked to *Microcodium* and bioturbating organisms. The red nuclei, which are observed in the large cylindrical rhizohaloes, are related to the filling by translocated clay material or clay illuviated by the surface horizons in the open hole of the rotting roots (Kovda and Mermut, 2010).

Impregnative redox features (Lindbo et al., 2010) are visible in thin section. They consist of small masses and nodules of amorphous pedofeatures of Fe/Mn oxides. The masses have amiboidal shape, diameter up to 0.9 mm, and diffuse or clear boundaries (Fig. 7D). Impregnative masses of Fe/Mn oxides are concentrated as coating or external hypo-coating pedofeatures around the rims of *Microcodium* (Fig. 6E) or of rare relict carbonate nodules (Fig. 7E) and internal hypo-coatings of subangular microaggregates (Fig. 6C). The Fe/Mn oxides nodules are subcircular; they have clear or diffuse boundaries (Fig. 7F).

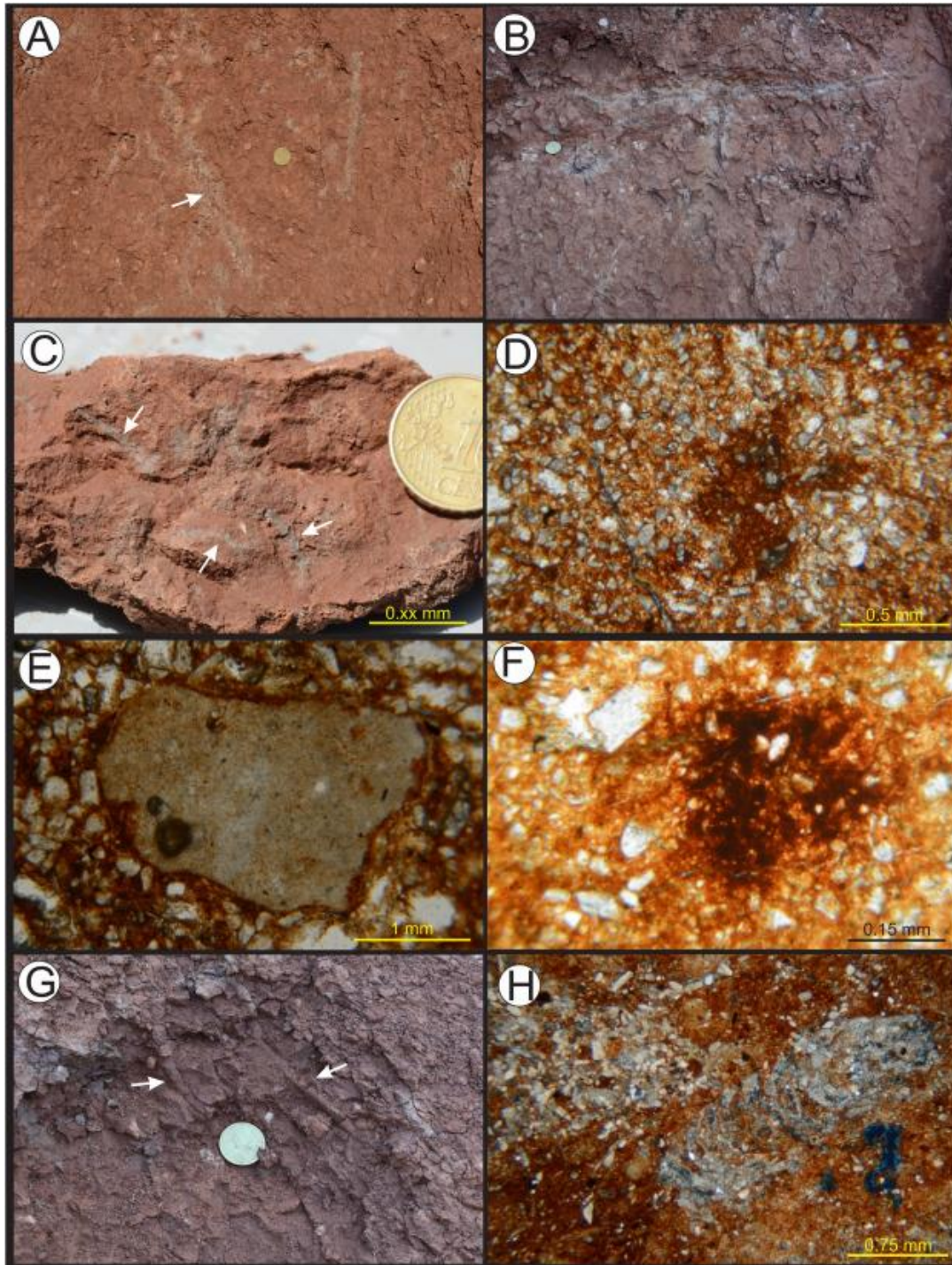


Fig. 7. Pont d'Orrit pedotype. Bss horizon. (A) Large cylindrical redox depletion features, interpreted as rhizohaloes (Kraus and Hasiotis, 2006). Note the greyish green edges and the weak red nucleus (see white arrow). Coin: c. 20 mm. (B) Large cylindrical redoximorphic feature in horizontal shape. The nucleus shows a red colour, which corresponds to material that fell felt down in the root hole from upper soil horizons. Coin, on left: c. 20 mm. (C) Small cylindrical redox depletions. They probably represent rhizohaloes produced by small size seasonal plants. Coin: c. 20 mm. (D) Amiboidal mass of redox concentration of Fe/Mn oxides. PPL. (E) Impregnative redoximorphic features of Fe/Mn oxide forming external hypo-coatings around a calcareous nodule. PPL. (F) Fe/Mn oxide impregnative nodule with diffuse boundaries. PPL. (G) Bioturbations take the form of cylindrical sandy mudstone tubular burrows, which are sub-vertical to the palaeosurface, 30–100 mm long and 3–15 mm in diameter. Coin: c. 20 mm. (H) Photomicrograph of crescent or bow-like fabric pedofeatures generated by bioturbation. XPL.

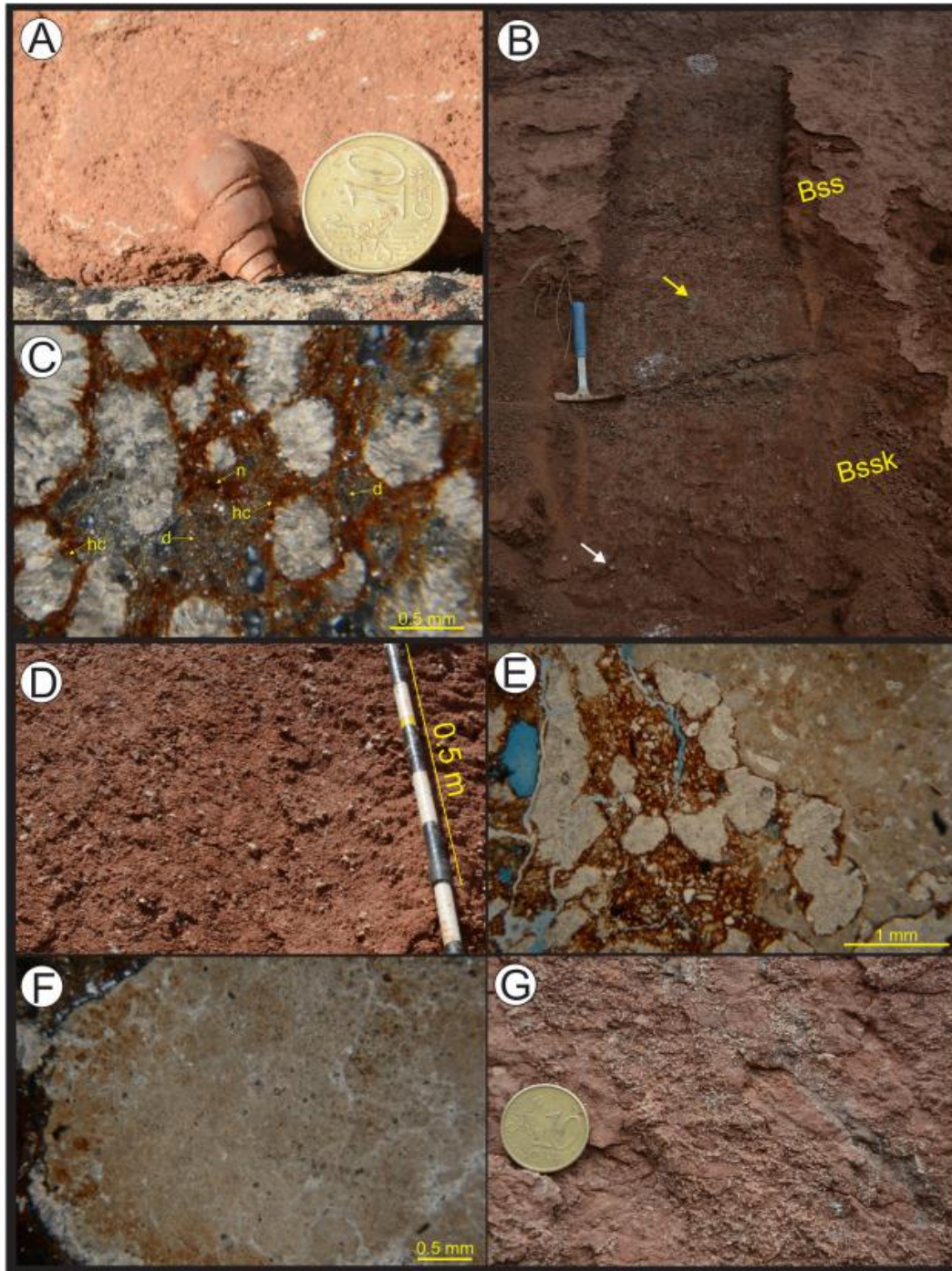


Fig. 8. Pont d'Orrit Pedotype. (A) Bss horizon. Fossil of a pulmonate snail, akin to *Vidaliella gerundiensis* (Vidal, 1883), common in Paleocene deposits of the Ebro Basin. Coin: c. 20 mm. (B) The diffuse transition from Bssk and Bss horizons is indicated by decreasing of the calcareous nodules (white arrow) and the increase of redox depletion (yellow arrow). The boundary is in correspondence of the bottom of the hammer. Hammer: 0.3 m. (C) Bssk horizon. Photomicrograph showing *Microcodium*, very abundant in this horizon, and typical stipple-speckled or mosaic-speckled b-fabric. Redoximorphic pedofeatures: (n) impregnative amorphous Fe/Mn oxides and (hc) Fe/Mn oxide external hypo-coatings, and (d) small areas of Fe/Mn depletion. XPL. (D) Bssk horizon. Isolated, small-sized, calcareous nodules in Bssk horizon. (E) Bssk horizon. *Microcodium* aggregates in contact with calcareous nodules seem to have dissolved the nodules during their formation. PPL. (F) Bssk horizon. Micritic calcareous nodule showing polygonal microfractures filled of microsparite. PPL. (G) Bssk horizon. Aggregates of *Microcodium* are very abundant in Bssk horizons. In places, redox depletions are localised around *Microcodium* aggregates. Coin: c.20 mm.

Carbonate nodules constitute less than 1% of the covered area. They are subspherical or ellipsoidal, have sharp boundaries and dimensions between 10 mm and less than 0.6 mm (Fig. 7E). Bioturbation is relatively common in this horizon. The burrows consist of sandy mudstone-filled cylindrical tubes, which are rectilinear or weakly arcuate, perpendicular to the bedding surface, 30–100 mm long and 3–15 mm in diameter; their external surface is characterised by thin ring-like relief, perpendicular to the cylinder axis. On the exposed area there are bioturbations between <1 to 5% (Fig. 7G). In thin section, the bioturbations appear as crescent or bow-like fabric pedofeatures (Fig. 7H). Moulds of gastropods, 22 mm long and 10 mm wide, are relatively common (Fig. 8A). They appear similar to the species *Vidaliella gerundensis* (Vidal, 1883) a Pulmonata snail that is typical of Paleocene continental deposits of the Ebro Basin (Gual i Ortí and Forner i Valls, 2013).

4.1.3. Bssk horizon

This horizon is made of the same parent material of the Bss horizon: a reddish brown (2.5YR 4/4) or red (2.5YR 4/6) poorly sorted, very fine-grained sandy mudstone. The thickness of the Bssk horizon is 0.5–1.9 m, and 1.14 m on average (Fig. 3A). The transition to the adjacent Bss or Ass/Bss horizons is indicated by a decrease of calcareous nodules and an increase of redox depletions (Figs. 8B and 9); the boundaries of this horizon have diffuse distinctness (0.15–0.4 m) and smooth, or rarely wavy, topography.

The coarse fraction of the groundmass consists of angular or subangular fragments of *Microcodium*, 0.08–0.12 mm in diameter, which varies in abundance between 20 and 40%, and reaches up to 80% in places. The c/f related distribution pattern is single spaced or close porphyric. Monocrystalline quartz clasts, up to 0.2 mm in diameter, are very rare (<1% in abundance). The dense micromass, 60–80% in abundance, is impregnated with a concentration of amorphous Fe/Mn oxides; planar voids are rarer than in the Bss horizon. The b-fabric, where visible under the Fe/Mn oxides covering, is stipple-speckled or mosaic-speckled (Fig. 8C).

Calcareous nodules are the distinctive characteristic of this horizon. The nodules are isolated and comprise 5–20%, on average 13%, of the exposed section area (Fig. 8D). They are subspherical or elongate, the diameter, or longer axis, varies from <1 to 40 mm across, and is on average c. 10 mm; the roundness is subangular or angular. In thin section, nodules are identified as typical crystalline pedofeatures. The nodules consist of very pale brown (10YR7/4) micrite; they are subrounded, equant or prolate, and show sharp or, in places, diffuse boundaries. Mamillate surface roughness is observable when they are in contact with aggregates of *Microcodium* (Fig. 8E). Internally they can show microfractures filled by microsparite which separate small polyhedral forms (Fig. 8F).

Smooth surfaces (slickensides) with striations and grooves are present also in this horizon; their dimension is smaller than 10 × 10 mm², and, in general, they are less common than in Bss horizons. They divide weakly developed very fine to fine (<10 to <20 mm in diameter) wedge-shaped structural aggregates.

Pedogenic impregnative redoximorphic features of Fe/Mn oxides are rare in this horizon. In thin section, they consist in small nodules of amorphous Fe/Mn oxides and in external hypo-coating of aggregates of *Microcodium* or of typical carbonate nodules (Fig. 8C). Greyish green (5G 5/2) redox depletions are distributed on the exposed surface of this horizon from 2 to 5% and, in general, are concentrated around the aggregates of *Microcodium* (Fig. 8G).

Aggregates of *Microcodium* are very abundant in this horizon; locally, they can cover 50% of the exposed area (Fig. 8G). Bioturbation traces are similar to those described in Bss horizon. Gastropods akin to the species *Vidaliella gerundensis* (Vidal, 1883) occur also in this horizon.

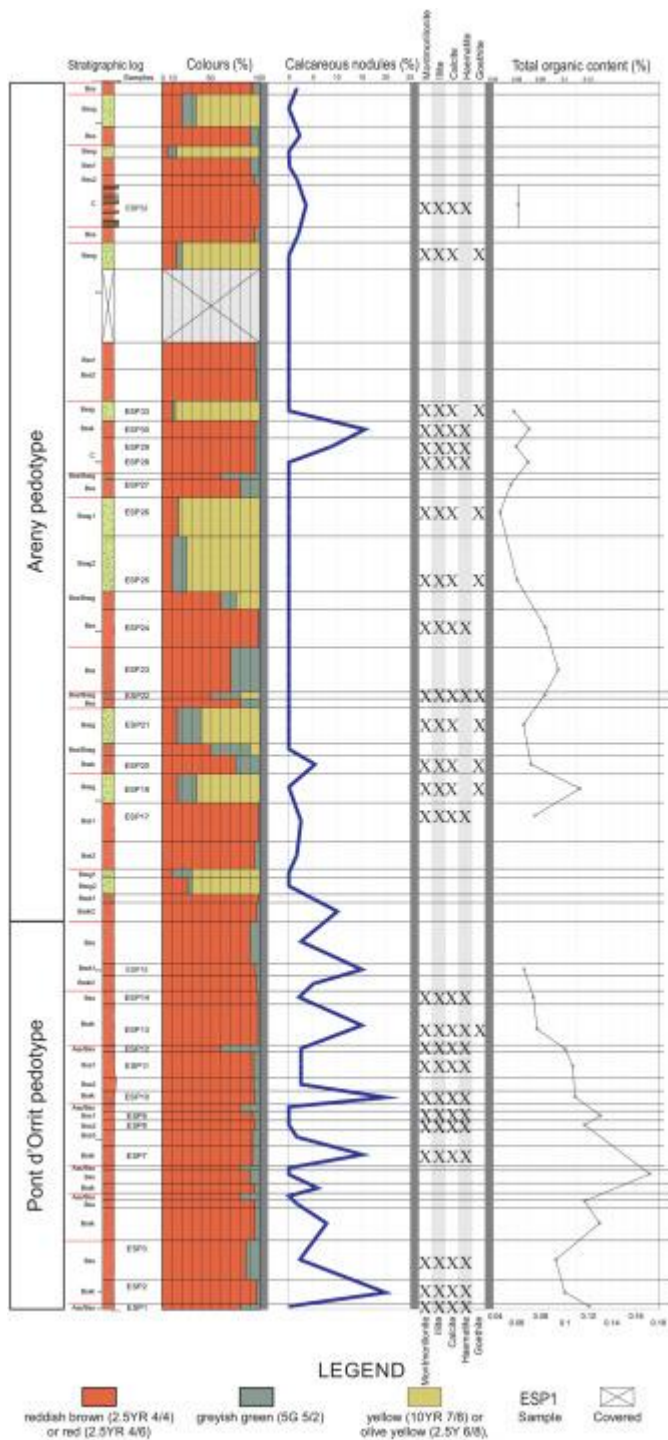


Fig. 9. Vertical distribution of abundance of colours, calcareous nodules, main minerals and total organic C content. Distribution of abundance of colours and calcareous nodules were measured in the field with a chart for estimating abundance; main minerals were determined by infrared spectroscopy; total organic C content was measured in the laboratory by combustion at 1150 °C using a TOC analyser. These characteristics allow differentiating the Pont d'Orrit from the Areny pedotype.

4.2. Areny pedotype

The upper portion of the study succession above the level 22.90 m from the base of the measured section (level 0 m) is dominated by the Areny pedotype (Fig. 2). This pedotype consists of profiles organised as follows (Fig. 3): the most common sequence of horizons is Bssg - Bss/Bssg - Bss - C; a less common one is Bssg - Bssk - C (see below for the horizon subdivision). The thickness of this pedotype varies between 0.9 and 8.85 m, and is on average 3.7 m. The horizons are present in the following percentages, bases on fraction of thickness: Bssg (37.3%), Bss (39.1%), Bss/Bssg (4.7%), Bssk (8.4%) and C (10.5%). The Bssg, Bss/Bssg and C horizons are described below; Bss and Bssk have the same characteristics of the profiles of the Pont d'Orrit pedotype.

4.2.1. Horizon Bssg

The parent material of this horizon is a dense sandy mudstone. The thickness varies from 0.35 to 3.3 m, the average is 1.55 m. The transition to the adjacent horizons is marked by an increase in reddish brown colour. Lower and upper boundaries exhibit diffuse distinctness (0.2 to 0.25 m) and smooth topography.

This horizon is characterised by variegated colours: yellow (10YR 7/8) or olive yellow (2.5Y 6/8), which constitutes 65–80% of the exposed surface; greyish green or pale green (5G 5/2 or 5G 6/2) (10–20% of the exposed surface); and reddish brown or dark reddish brown (2.5YR 4/4 or 2.5YR 3/4) (10–15% of the exposed surface) (Fig. 10). The coarser portion of the groundmass (Fig. 11A) consists of: (i) disarticulated subangular fragments of *Microcodium* (0.08 to 0.24 mm in diameter), the abundance of which is 15–20%; (ii) angular calcareous nodules (0.6–2.5 mm), less than 2% in abundance, showing sharp and corroded margins; (iii) angular quartz grains (0.08 to 0.16 mm), with abundance of less than 1%. The micromass is formed of dense clay-size material, consisting of montmorillonite. In thin sections, under plane polarised light (PPL), the micromass is olive yellow (2.5Y 6/8) and it constitutes 80% of this horizon. Concentrations of amorphous Fe/Mn oxides cover 10–15% of the surfaces. The c/f related distribution pattern is open or double-spaced porphyric (Fig. 11A). The b-fabric is stipple- or mosaic-speckled (Fig. 11A).

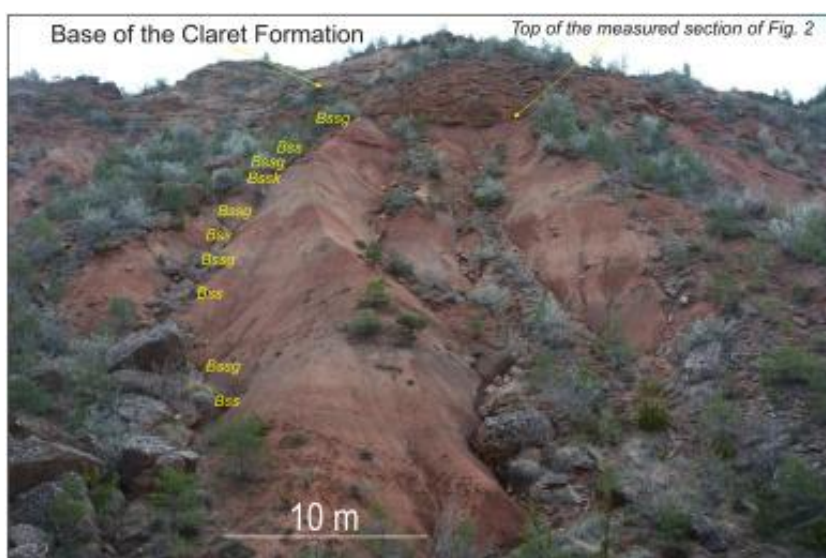


Fig. 10. Photograph of the upper portion of the measured section, which is characterised by the Areny pedotype. Some horizons of this palaeosols are indicated in figure. At the bottom the width of view is c.40 m.

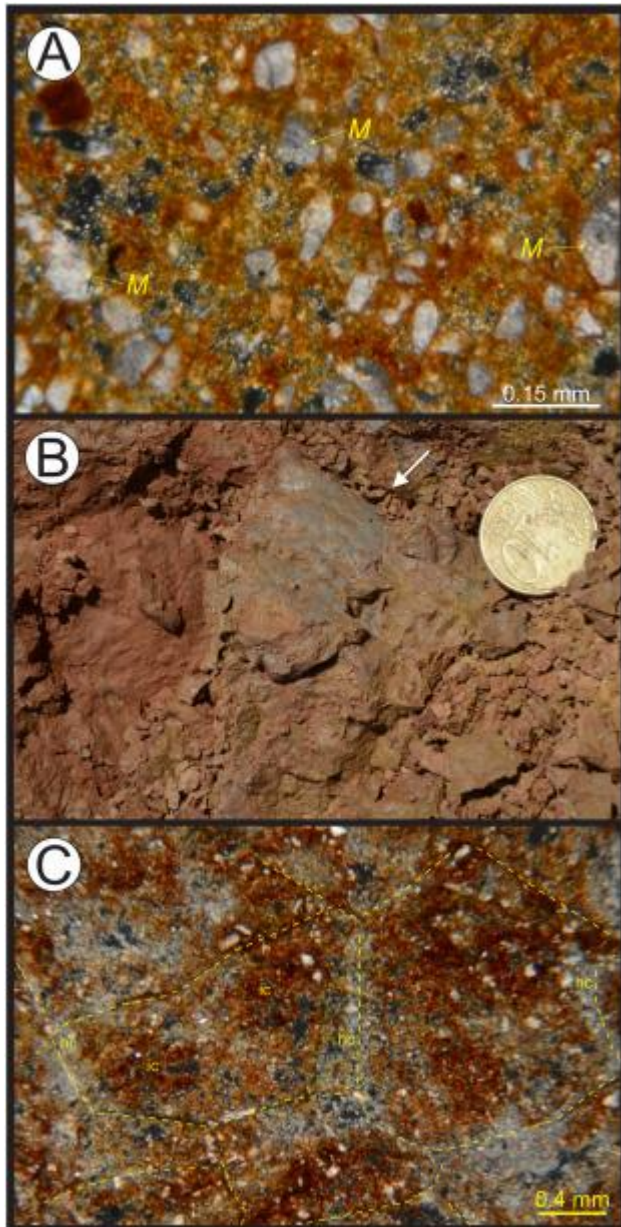


Fig. 11. Areny pedotype. (A) Photomicrograph of Bssg horizon. Coarse portion of the groundmass is constituted almost exclusively of fragments of *Microcodium* (M). The b-fabric is typically stipple- or mosaic-speckled and the c/f related distribution pattern open or double-spaced porphyric. XPL. (B) Slickenside surface (white arrow) on Bssg horizon showing greyish green redox depletions and yellow redox concentrations. Coin: c.20 mm. (C) Photomicrograph of very fine angular blocky peds. Note the redoximorphic greyish green depletion as internal hypo-coating (hc) of the angular blocky peds and the reddish brown redoximorphic impregnative concentration (ic) in their internal part. Yellow stippled lines outline the microped margins. XPL.

Smooth surfaces (slickensides), up to $40 \times 40 \text{ mm}^2$, showing striations and grooves and red, yellow, olive yellow and greyish green redoximorphic features (Fig. 11B), separate medium-size (20 to 50 mm in diameter) wedge-shaped structural aggregates. In thin sections, very-fine (2–3 mm across) angular blocky peds are separated by thin planar voids (Fig. 11C). Overall, the grade of pedality is from moderately to strongly developed. Greyish green redox depletions form internal hypo-coatings of the angular blocky micropeds and their internal part is characterised by amiboidal impregnative redox masses up to 0.5 mm in diameter (Fig. 11C).

Under suitable exposure conditions, it is possible to observe a typical morphology named “bowl structure” (Eswaran and Cook, 1988; Lynn and Williams, 1992; Ahmad and Mermut, 1996; Schoeneberger et al., 2012). In Fig. 12, the topmost Bssg horizon shows a concave upwards structure, referred to as “bowl”, bounded at the bottom by spoon-shaped master slickensides, and characterised inside by wedge-shaped structures (mukkara structure).

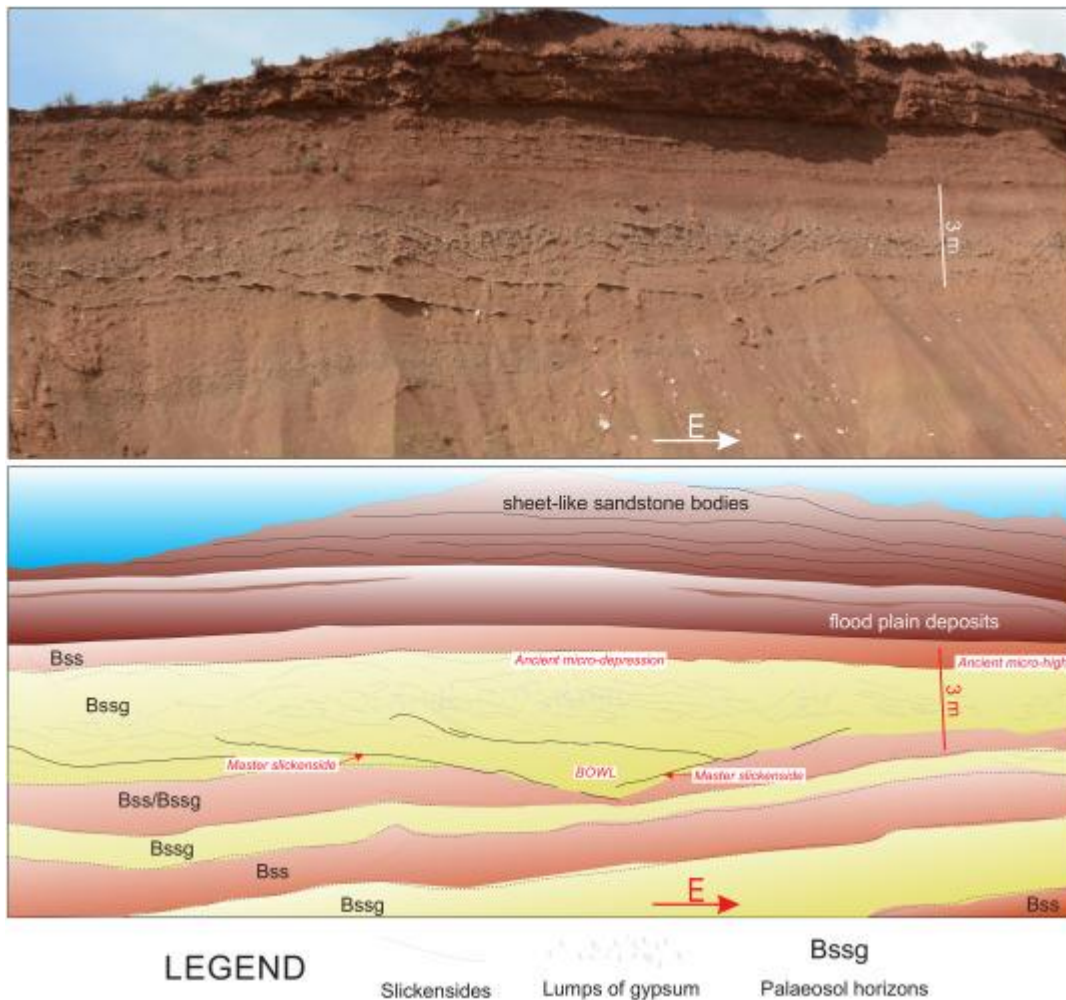


Fig. 12. Areny pedotype. The “bowl structure” is a typical characteristic of Vertisols, formed by swelling and shrinking processes, which on the surface of the soil corresponds to micro-depressions separated by micro-highs. This three-dimensional alternation of micro-depressions and micro-highs constitute the micromorphology named “gilgai”. Note the master slickenside separating the bottom of the bowl structure and the accumulation of lumps of gypsum in Bssg horizon.

In places, this horizon exhibits vertical and planar, or slightly sinuous, bands (>1.5 m high and >1 m wide), which are narrow (30–40 mm thick) and nearly perpendicular to the strata. These features display irregular pale green (5G 6/2) margins and inside contain reddish brown (2.5YR 4/4) “mottles”, aligned along the planar zone and <10–50 mm across (Fig. 13A). Similar features were described in ancient and modern soils (Joeckel et al., 2017, their Fig. 14A and B; Dudek et al., 2019, their Fig. 3B) and can be interpreted as filled and sealed cracks. The pale green colour is due to redox depletion by stagnant water, where the reddish brown “mottles” probably represent surface soil material that intruded along the open fracture (Joeckel et al., 2017; Dudek et al., 2019).

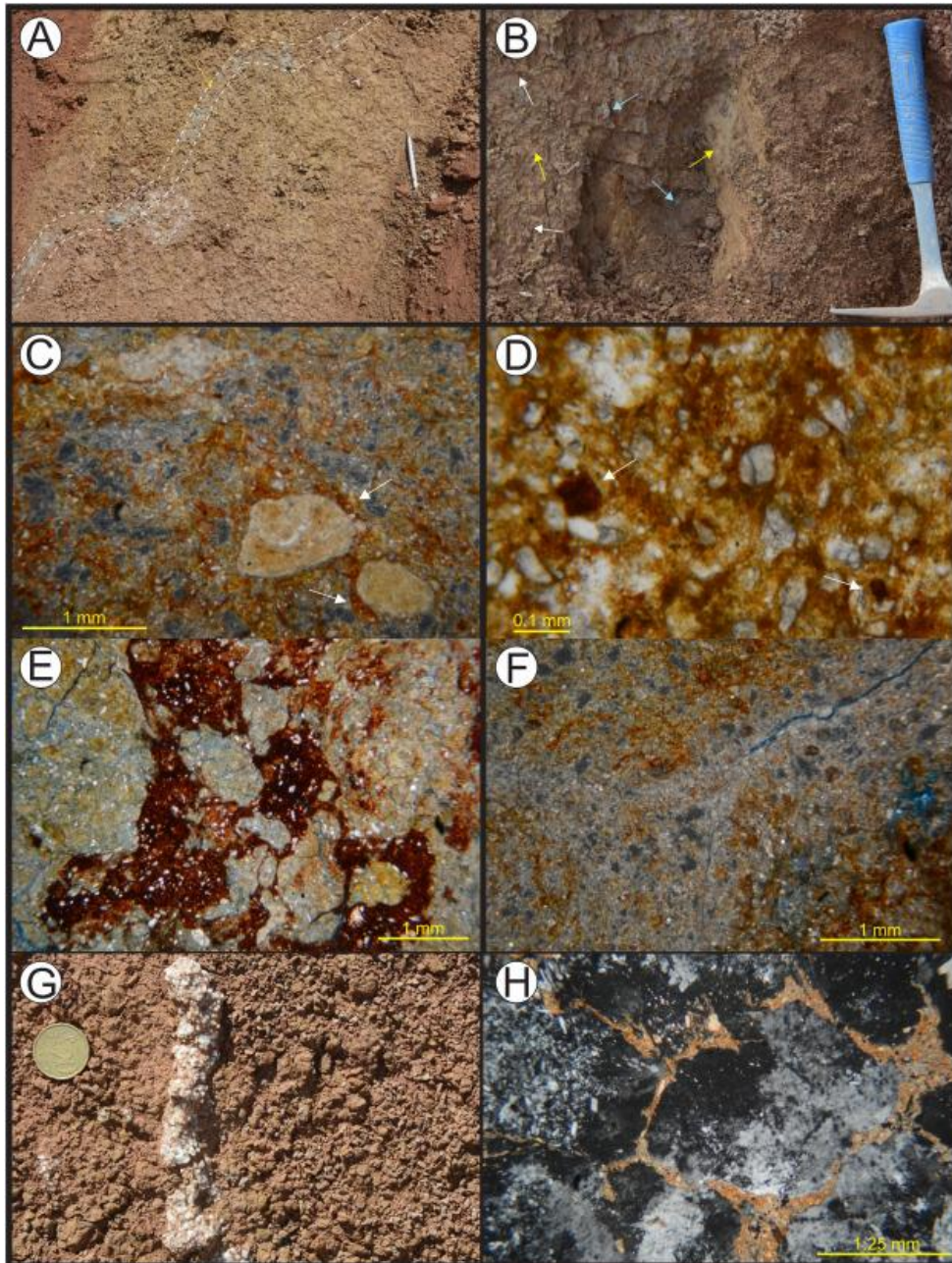


Fig. 13. Areny pedotype. (A) Narrow (30–40 mm) vertical planar zone (indicated by white dashed line on an undulated exposure surface), more than 1.5 m high and more than 1 m wide, displays pale green redox depletion margins (black arrows) and reddish internal portion (yellow arrow). This structure is interpreted as a vertical crack, into which stagnant waters caused redox depletion of the of the internal walls at the beginning of the wet season and into which reddish oxidised material fell during the dry season. Note the yellow or olive yellow colour of the palaeosol matrix which corresponds to goethite concentration. Clutch pencil: 142 mm. (B) Typical colour variety of Bssg horizon. Yellow or olive yellow dominant colour corresponding to goethite (yellow arrows); greyish green bodies (mottles) indicating depletion areas (blue arrow); reddish brown bodies (mottles) which are the original colour of the parent material containing haematite (white arrow). Hammer: 0.3 m. (C) Bssg horizons. Impregnative Fe/Mn compounds as external hypo-coating of calcareous relict nodules. XPL. (D) Bssg horizon. Impregnative redox Fe/Mn nodules. PPL. (E) Bssg horizon. Impregnative redox Fe/Mn masses on groundmass filling cracks. PPL. (F) Bssg horizon. Redox depletion around a small rhizohalo. XPL. (G) Bssg horizon. Lump of gypsum, perpendicular to the bedding surface, probably constituting filling of root holes. Coin: 22.25 mm. (H) Bssg horizon. Photomicrograph of a lump of gypsum. Note the sandy mudstone squeezed by the displacive growth of the gypsum. XPL.

In the field, other redoximorphic features include (i) intense concentrations of yellow or olive yellow Fe/Mn compounds (goethite, see below) (Fig. 13A) and (ii) redox depletions characterised by small irregular shape, greyish green bodies, 10–30 mm across (Fig. 13B). In thin section, impregnative redox Fe/Mn compounds are observed as external hypo-coating of calcareous nodules (Fig. 13C), Fe/Mn nodules, 0.15–0.3 mm across (Fig. 13D), and masses inside filled cracks (Fig. 13E). In thin sections, other redox depletions can be observed as small rhizohaloes (Fig. 13F) and Fe/Mn oxide reduced groundmass (Fig. 13C).

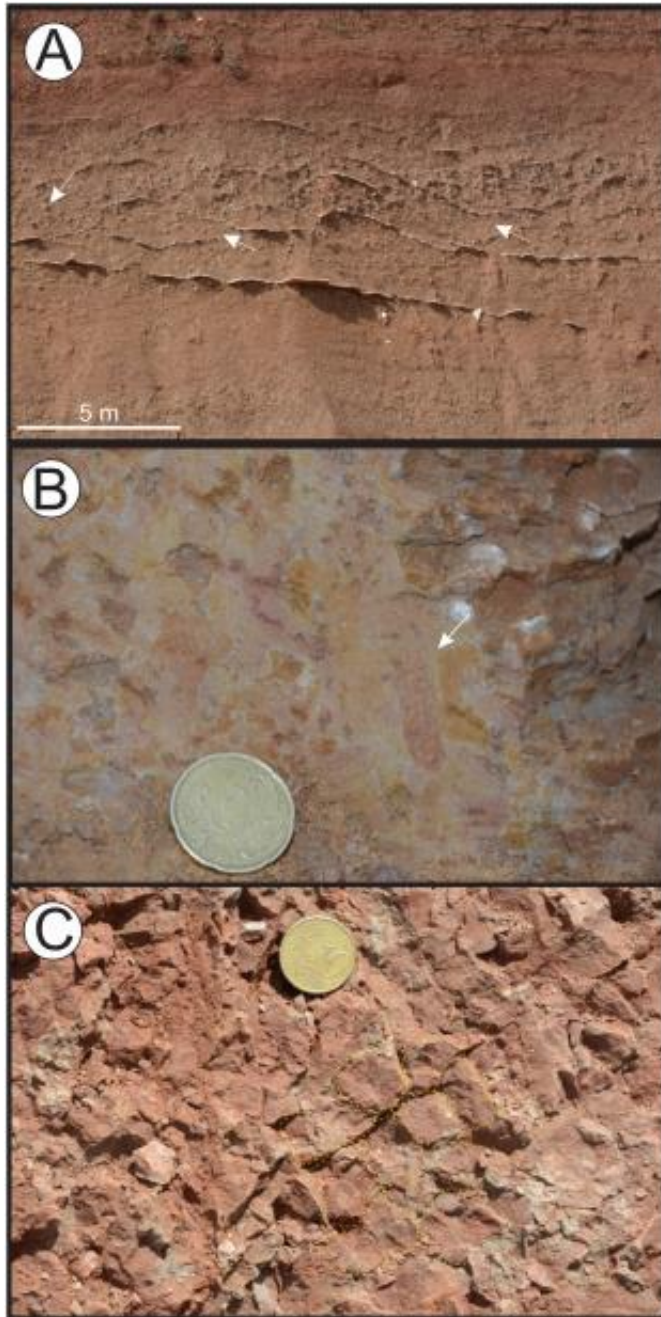


Fig. 14. Areny pedotype. (A) Bssg horizon. Prismatic gypsum precipitated into open slickenside fractures during the pedogenesis. The white lines allow to easy identifying a typical mukgara structure of Vertisols. Lumps of gypsum are arrowed. At the bottom the width of view is c. 20 m. (B) Bssg horizon. Redox depletion as external hypo-coating around a bioturbation. Coin: 22.25 mm. (C) Moderately developed angular blocky peds (locally indicated by yellow dashed lines) in Bss/Bssg horizon. Coin: c. 20 mm.

Lumps of gypsum and gypsum filling planar slickenside fractures are exclusive of this horizon. Lumps have a prolate form, with a long axis that tends to be perpendicular to the bedding surface, up to 150 mm long and up to 70 mm wide (Fig. 13G). The gypsum crystals are white and opaque and are separated by thin mudstone streaks. In thin section, the gypsum appears as consisting of poorly defined interlocking macrocrystals, 1.6 to 4.8 mm in size, and of disorganised masses of prismatic microcrystals, 0.08–0.32 mm long, amongst which small portions of the soil material appear squeezed (Fig. 13H). Gypsum filling planar slickenside fractures is 1–10 mm thick, has prismatic form and it is made of crystals that are perpendicular to the slickensides planes. Sometimes this permits a clear identification of the mukara structure (Fig. 14A).

Aggregates of *Microcodium* are extremely rare or absent. Bioturbation consists of vertical cylindrical burrows, 10 mm high and 3 mm wide, commonly showing redox depletion at their external margins (Fig. 14B). In thin sections, crescent or bow-like fabric pedofeatures are relatively frequent.

4.2.2. Horizon Bss/Bssg

This horizon has the same parent material as horizon Bssg and exhibits characteristics that are intermediate between those of Bss and Bssg. Its thickness is 0.4–1 m, on average 0.7 m, and the dominant colour is reddish brown (2.5YR 4/4) (c. 60% of the exposed surface), whereas greyish green (5G 5/2) and olive yellow (2.5Y 6/8) colours represent c. 25% and 15%, respectively, of the exposed surface. It is noted that the olive yellow or yellow colours are always transitional between reddish brown and greyish green colours. The transition to the adjacent Bssg or Bss horizons is characterised by a diffuse distinctness (0.2 m) and smooth topography. Smooth surfaces (10 × 10 mm²) separate wedge-shaped, parallelepiped-shaped and moderately developed angular blocky peds (Fig. 14C). Aggregates of *Microcodium* are absent.

4.2.3. Horizon C

In the studied interval, only two C horizons are identified, which are 2.1 and 2.5 m thick (Fig. 2). The distinctness of the lower boundary is sharp, whereas the upper boundary is diffuse; the topography is smooth. Where tabular sandstone strata are interlayered to reddish brown (2.5YR 4/4) sandy mudstone, the C horizon can be readily distinguished macroscopically (Fig. 15A). In the other cases, the absence of pedogenic features (e.g., smooth surfaces, redoximorphic features, pedogenic structures) and the microscopic analyses of thin sections permit their identification. De facto, in thin section, it is possible to observe sedimentary structures that consist of coupled laminae with crude grading (0.4–0.8 mm thick). The lower lamina, 0.24–0.64 mm thick, is constituted of disaggregated fragments of *Microcodium* (0.05–0.15 mm in diameter and frequency 60–90%) and calcareous nodules (c. 0.15 mm in diameter and frequency 20–30%). The upper lamina, 0.16 mm thick, is formed of mudstone material with few fragments of *Microcodium* (frequency 10–15%) (Fig. 15B). Some elongated grains display the long-axis orientated parallel to the bedding surface. The laminae have sharp or clear contacts, a lateral extent greater than 40 mm, and common thickness variations. Corn-cob and rosette aggregate forms of *Microcodium* are abundant in this horizon; these structures cross the laminae interrupting their lateral continuity (Fig. 15C).

The C horizon is considered the parent material of the palaeosol, since it exhibits the same texture and overall mineralogical characteristics (see below) of the B horizons and contains preserved sedimentary structures.

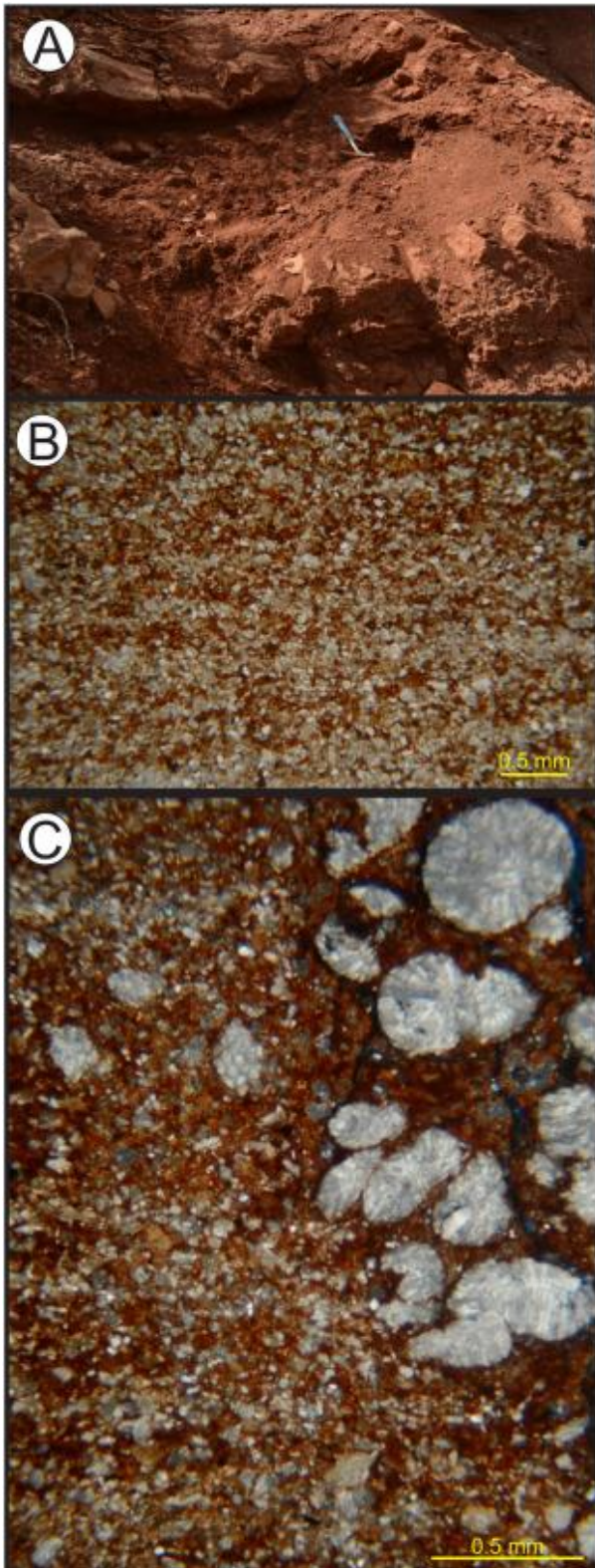


Fig. 15. Areny pedotype. (A) C horizon that is macroscopically distinguishable by the presence of thin sandstone beds. Hammer: 0.3 m. (B) C horizon that is constituted of sandy mudstone and that can be distinguished by other horizons by the absence of pedogenic features and, in thin section, by the presence of sedimentary structures as observed in this photomicrograph. (C) Aggregates of *Microcodium* cross-cutting the sedimentary structures in a C horizon, which are the only effect of pedogenesis.

4.3. Distribution of minerals and organic matter

Infrared spectrometric analyses recognised the following main minerals: montmorillonite, illite, calcite, haematite and goethite (Fig. 9, Fig. 16). Three minerals are the most common across all the horizons: montmorillonite, illite and calcite (Fig. 16). Montmorillonite is dominant in the spectral mixture, varying from 45 to 65% of these three minerals; the proportion of illite is 22 to 40%; that of calcite is 16 to 28%. It is worth noting that the relative distribution of these minerals is similar in all the horizons, and in particular even in C horizons, where the pedogenesis is considered to have been minimal (Fig. 16). Overall, the clay analyses align with the clay-mineral stratigraphy of Schmitz and Pujalte (2003) (their Fig. 2), although these authors also recognised a limited presence of kaolinite and chlorite. Calcite is abundant in all the horizons (Fig. 16), as noted in the micromorphological analyses. Calcite occurs as fragments of *Microcodium*, aggregates of *Microcodium* and calcareous nodules. Fragments of *Microcodium* are present in all the horizons, including the C horizons, revealing that they are part of the parent material. Aggregates of *Microcodium* with corn-cob or rosette forms are viewed as pedogenic. Well-sorted, very small (max 0.15 mm across) calcareous nodules occur in C horizons; they are considered as part of the parent material. Fig. 9 emphasises the abundance of the calcareous nodules on the exposed surface. Haematite and goethite are unevenly distributed in the horizons. Haematite occurs exclusively in Bss, Bssk, Ass/Bss and C horizons, while it does not appear in Bssg horizons where goethite dominates (Fig. 9, Fig. 16). In Bss/Bssg horizons haematite and goethite are both present in similar proportions.

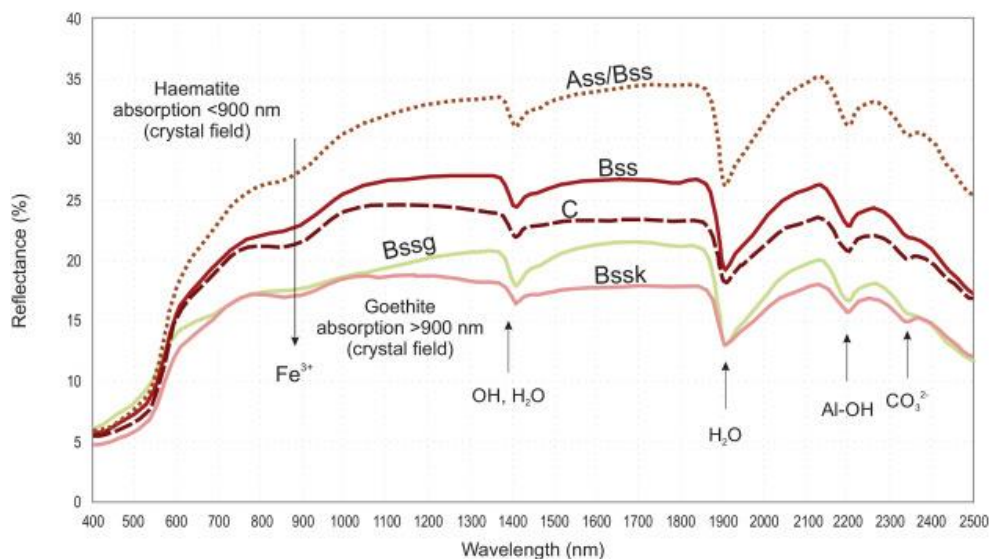


Fig. 16. Infrared spectroscopy diagrams of the main minerals of the palaeosol horizons of the Esplugafreda Formation. The palaeosol horizons Ass/Bss, Bss, Bssk, Bssg and C correspond to the samples ESP12, ESP9, ESP13, ESP25 and ESP 32 respectively. See Fig. 2. Clay spectral features are present in the SWIR (shortwave infrared region: 1000–2500 nm) at 1400 nm, 1900 nm and most importantly between 2100 and 2500 nm. Clays exhibit several spectral features, which result from the presence of vibrational hydroxyl processes. Montmorillonite is characterised by asymmetric absorption bands at ~1400 nm (OH; H₂O), ~1900 nm (H₂O – deep feature) and 2200 nm (Al-OH). Illite shows symmetric absorption features at ~1400 nm (OH), ~2200 nm (Al-OH). Calcite has strong absorption bands corresponding to the vibrational modes of CO₂–3 ions between 2340 and 2345 nm. Iron oxides and hydroxides display features in the VNIR (visible near infrared: 400–1000 nm) range. The main Fe absorption occurs at 900 nm (crystal field feature). Haematite usually has a narrower absorption at a shorter wavelength than goethite. Considering the SWIR features, all the horizons are dominated by montmorillonite, illite and calcite. VNIR features indicate a prevalence of haematite in all the horizons with the exception of Bssg, in which it is substituted by goethite.

The total organic carbon content (TOC) varies from 0.04 to 0.17% (Fig. 9). The palaeosol profiles of both pedotypes do not exhibit a regular trend of organic carbon distribution. The C horizon, which is considered to have characteristics that are close to those of the parent material, shows a similar amount of TOC to that of the other horizons (0.06–0.07%).

5. Discussion

5.1. The subdivision of the palaeosol profiles

The palaeosol profiles (pedons) are not easy distinguishable at first sight (Soil Survey Staff, 1999; Buol et al., 2011). De facto, elements such as interbedding of deposits with preserved sedimentary structures or erosional surfaces, which allow distinction of different palaeosol profiles, are absent. On the contrary, almost all the palaeosol horizons demonstrate gradual transitions between them (diffuse distinctness). For this reason, internal macroscopic and micromorphological characteristics, and transition statistics describing the vertical superposition of the horizons (see Supplementary Material 1) were used to define the organisation of the palaeosol profiles. According to internal macroscopic and micromorphological characteristics: (i) Ass/Bss horizons, which show higher distribution of redox depletion features attributable to rhizohaloes (Kraus and Hasiotis, 2006), occur in the topmost part of the palaeosol profile; (ii) Bssk horizons, which contain calcium carbonate nodules attributable to leaching, are placed in the lower part of the profile (Mermut et al., 1996b; Elias et al., 2001a); (iii) Bssg horizons, showing redoximorphic features attributable to surface-water gley (PiPujol and Buurman, 1994) (see below), are placed in the upper part of the profile; and, (iv) consequently, the Bss horizon is placed at an intermediate position between Ass or Bssg above and Bssk or C below. Analysis of vertical transition statistics of the horizons, based on the application of Markov chain analyses (see Supplementary Material 1), confirms this style of juxtaposition of the horizons in both pedotypes. According to these considerations, as described above, the Pont d'Orrit pedotype is characterised by the sequence of horizons Ass/Bss-Bss-Bssk, whereas the Areny pedotype is characterised by the sequence of horizons Bssg-Bss/Bssg-Bss-(Bssk)-(C).

5.2. Taxonomy and genetic characteristics of the two pedotypes

5.2.1. Taxonomic classification

The Table 1 summarises the main similarities and differences in the characteristics of the Pont d'Orrit and Areny pedotypes.

The high content of montmorillonite clay, the high density of the matrix, and the presence of slickensides, wedge-shaped structural aggregates, mukgara and bowl structures are typical characteristics that permit classification of these pedotypes as Vertisols (Soil Survey Staff, 1999, Soil Survey Staff, 2014; Ahmad, 1983; Mack et al., 1993; van Breemen and Buurman, 2002). Some other typical characteristics of the Vertisols, though not necessarily restricted to these, are (i) heterogeneous groundmass, (ii) porphyric c/f related distribution pattern, (iii) stipple- and mosaic-speckled b-fabric and (iv) low organic C content (TOC).

Heterogeneous groundmass consists of material that was originally extraneous to the horizon and that fell from upper horizons into cracks (Fig. 13A) or holes left by decaying roots (Fig. 7A and B) (Joeckel et al., 2017; Dudek et al., 2019). The porphyric c/f related distribution pattern reflects high quantities of micromass contained in the palaeosols. Stipple- and mosaic-speckled b-fabric is related to random distributed patches of clay minerals. These two latter characteristics are commonly

described in Vertisols (Kovda and Mermut, 2010). Modern Vertisols contain low quantities of organic carbon, in general <2% (McGarry, 1996; Elias et al., 2001a; van Breemen and Buurman, 2002); ancient Vertisols contain even less (e.g., Gastaldo et al., 2020), as observed in samples from the Esplugafreda Formation. The irregular distribution of the organic carbon within the palaeosol profiles (Fig. 9.) can be explained in part by pedoturbation, and in part by the fact that the palaeosols are cumulative in nature (see below), which prevents the development of a systematic trend of the organic C in the soil profile.

5.2.2. Types and maturity of the palaeosols

Catt (1990), Marriott and Wright, (1993; see their Fig. 4) and Kraus, (1999; see her Fig. 2), amongst many others, have shown that in sedimentary successions characterised by palaeosols the processes of erosion, deposition and stasis (or sediment bypass) generate different types of organisation of palaeosol profiles. Marriott and Wright (1993) distinguished compound, cumulative, polygenic and composite palaeosol profiles. Compound palaeosols are separated by sediments not affected by pedogenesis. They are formed by episodic and rapid depositional processes leading to the accumulation of material that is sufficient to bury the underlying soil and interrupt its development. Cumulative palaeosol profiles are generated by slow and continuous sedimentation, which permits the incorporation of more recently deposited sediment into the soil without interrupting its development. The boundaries of cumulative palaeosol profiles are not marked by deposits or erosional surfaces, but they have a diffused continuity, and the horizons can be exceptionally thick. Polygenic palaeosols develop on static depositional surfaces where environmental changes overprint the same horizon with different pedogenic characteristics. Composite palaeosols are affected by rapid and episodic sedimentation processes, but the deposits are not so thick as to completely bury the underlying soil; thus overlapping horizons occur.

Most of the palaeosol profiles of the Esplugafreda Formation are cumulative. Continuous and relatively rapid sedimentation caused the generation of diffuse boundaries between the palaeosol profiles and horizons thicker than 1 m. For example, in modern Vertisols slickensides and related wedge-shaped features develop in Bss horizon up to 1.5–2 m from the soil surface, because at greater depth moisture variations that would drive shrinking and swelling processes are limited (Yaalon and Kalmar, 1978; Mermut et al., 1996a; van Breemen and Buurman, 2002). Conversely, the horizons with slickensides of the Esplugafreda Formation reach almost 7 m of thickness, indicating a progressive accretion of the soil during its formation. What was the sedimentation rate of the Esplugafreda Formation floodplain? Daniels (2003) demonstrated that the maximum aggradation rate that would allow pedogenesis to keep up with sedimentation is ~0.5 mm/y. This value is compatible with estimates for the Esplugafreda Formation (see below calculations based on the size of the calcareous nodules; Retallack, 2005); however, the amount and frequency of the sedimentary input should have been variable through time in order to allow formation of well-defined horizons (Bss, Bssk, Bssg) and palaeosol profiles of different thickness.

In the Esplugafreda Formation, only two compound palaeosol profiles have been observed, both belonging to the Areny pedotype and located in the upper part of the study section (Fig. 2). These profiles display a C horizon characterised by relics of sedimentary structures, and which sharply overlies cumulative profiles. This type of palaeosol profile indicates that the rate of sediment supply and deposition were - at that point in time and space - sufficient to bury the underlying soil and stop its development.

Table 1. Summary of similarities and differences of the pedotypes of the uppermost part of the Esplugafreda Formation. C: common (in all the palaeosol profiles); R: rare (present in few palaeosol profiles); A: absent (completely absent in any palaeosol profile).

Characteristics of the horizons of the two pedotypes Pedotype	PONT D'ORRIT	ARENY
<i>Macroscopic characteristics</i>		
High density parent material	C	C
Parent material composed of up to 80% of fine grained material (<62 µm)	C	C
Very few (<5%) voids	C	C
Slickensides	C	C
Angular blocky and wedge-shaped structures	C	C
Bowl-like structure, separated by master slickensides	C	C
Mukkara structure	C	C
Monotonous and dominant reddish brown colour	C	C
Weak characterisation of the horizons	C	R
Transition between horizons with diffuse distinctness and smooth topography	C	C
Local heterogeneous element in the groundmass	C	C
Rhizohaloes	C	C
Disaggregated fragments of Microcodium	C	C
Calcareous nodule	C	C
In situ lumps of gypsum	C	R
Reddish brown (2.5YR 4/4) or red (2.5YR 4/6)	A	C
Yellow (10YR 7/8) or olive yellow (2.5Y 6/8)	C	R
More than 0.5 m long sealed cracks	A	C
<i>Palaeontological characteristics and organic C content</i>		
Bioturbation	C	C
Molds of gastropods	C	C
Corn-cob and rosette aggregates of Microcodium	C	R
Low and irregular distribution of organic C content	C	C
<i>Micromorphological or microstructural characteristics</i>		
Subangular or angular blocky micropeds	C	C
Local cracks, characterised by redox depletion	A	C
C/f (coarse/fine) open or double-spaced porphyric related distribution pattern	C	C
Stipple-speckled or mosaic-speckled b-fabric	C	C
Impregnative redox Fe/Mn nodules or mass	R	C
Local heterogeneous element in the groundmass	C	C
Alternating laminae of fine- to very fine-grained sand (C horizon)	A	R
<i>Mineralogical characteristics</i>		
High content of montmorillonite clays	C	C
Haematite	C	C
Goethite	A	C

In cumulative soils of the Esplugafreda Formation, the continuous accretion of the soil surface led to the generation of poorly developed soils. In parallel, several other aspects of the palaeosols of the Esplugafreda Formation are indicative of short development time. Bssk horizons consist of isolated calcareous nodules (5–30 mm across), which are comparable with stage II calcareous horizon (Gile et al., 1966; Machette, 1985; Zamanian et al., 2016), whose age of development varies according to

Machette (1985) between 10 and 200 ky. In addition, the application of an empirical relationship by Retallack (2005), according to which the size of the calcareous nodules is a function of time ($A = 3.8250.34$, where A is age in ky and S is the largest diameter of carbonate nodule in centimetres - 40 mm in Bssk horizon), shows that the Esplugafreda calcareous nodules, and consequently the palaeosol profiles with Bssk horizons, may have developed over c. 6.3 ky. Considering the mean thickness value of the Pont d'Orrit profile (3.2 m), the calculated sedimentation rate (~ 0.507 mm/y) approximates the value indicated by Daniels (2003) as that associated with the maximum accretion rate that would allow pedogenesis to keep up with sedimentation (see above). The short development time of horizons, due to the continuous accretion of topographic surfaces, can probably be inferred by the irregular distribution of organic carbon in palaeosol profiles because of the relatively long time required for the distribution of organic matter according to a trend.

The C horizons allow some consideration of the depositional processes that occurred in the ancient floodplain. Very thin (0.24–0.64 mm thick) laminae of fine-grained sands grading to mudstone and the absence of structures suggesting bedload transport (like current ripples) indicate deposition from settling from low-energy (low stream power) subaqueous turbulent suspensions. The abundant occurrence of montmorillonite and haematite in C horizons (Fig. 16), i.e. in the floodplain deposits without palaeopedogenic alterations, is evidence of the detrital origin of these two mineral components in the parent material of the palaeosols.

5.2.3. Climatic aspects

Vertisols are soils not associated with a particular climate. Vertisols occur in extremely varied climate conditions: from equatorial (hyperthermic soil temperature regime) to cold (cryic soil temperature regime) through monsoonal tropical, semi-arid, dry Mediterranean and sub-humid temperate (Ahmad, 1983; Ahmad and Mermut, 1996; Soil Survey Staff, 1999). However, two climatic factors are important for the genesis and development of Vertisols: temperature and pronounced periodic precipitations, which control well-defined wet and dry cycles. Temperature is important for the in-situ production of smectitic clays from parent rocks (e.g., basalt) (Mermut et al., 1996a). Yet, this factor is not relevant for the Esplugafreda Formation, because the montmorillonite is clearly detrital, as testified by the interlayered deposits (C horizons), which contain high quantities of this clay. Thus, the most important climatic control on the formation of Vertisols in the Esplugafreda Formation was well-defined wet/dry periods, which caused alternating humidification and drying of the soil and the consequent swelling and shrinking of expandable clays. On the top surface of Vertisols, these effects resulted in the formation of cracks; in the subsoil, instead, the formation of cleavage planes and polished faces (slickensides) lead to separation of wedge-shaped or angular blocky peds. These soil structures originated from overburden pressure and stress associated with the alternating phases of swelling and shrinking (Ahmad, 1983). Slickensides are the sub-surface expression of the surface soil cracks, as the deeper portion of the cracks is tightly connected with the upper vertical terminus of the slickensides (Lynn and Williams, 1992). The intensity of the cracks, i.e. the number of the cracks per area and volume of the soils (Ahmad, 1983), is directly associated with the intensity of the slickensides, i.e. the number of slickensides per area and volume, in subsurface soil horizons. This means that in the subsoil, the small wedge-shaped or blocky peds, separated by slickensides, correspond to intense cracking at the soil surface. Yong and Warkentin (1966) observed that the intensity of cracking increases with the increase of soil moisture, but that cracking is particularly more intense when the moisture difference between the wet and dry season is well defined. Elias et al. (2001b) observed that Vertisols of the alluvial plain lying between the White and Blue Nile (Gezira area, Sudan) exhibit an increase in superficial crack intensity from the drier northern areas (200

mm/y) towards the more humid southern areas (450 mm/y). This trend is accompanied by the disappearance of gypsum crystals in groundmass, the appearance of carbonate nodules in the soil profile and an increase of clay content in the parent material. The Gezira area is characterised by a marked seasonal variation of precipitation, concentrated in summer months. By analogy, the two pedotypes of the Esplugafreda Formation, which are characterised by high intensity of slickensides, small wedge-shaped and angular blocky aggregates, and high amount of clay minerals, can be associated with a palaeoclimate characterised by the alternation of well-differentiated drier and wetter seasons.

5.2.4. Vegetation cover

In modern Vertisols, the vegetation cover is strongly controlled by the marked alternation of dry and wet periods, the shrinking and swelling processes and the high clay content. This causes the limited development of vegetation, such that the most common environments overlying these soils are grasslands and savannahs (Dudal, 1963; Ahmad, 1983; Coulombe et al., 1996; Mermut et al., 1996a, Mermut et al., 1996b; Elias et al., 2001a). Most vegetation is seasonal grass, and the few trees are characterised by deep roots that allow them to overcome droughts and the root damage caused by the shrinking and swelling processes, which act up to a depth of 1.5–2 m from the surface (Lynn and Williams, 1992; Mermut et al., 1996a, Mermut et al., 1996b). In the Esplugafreda Formation, rhizohaloes are the only record of vegetal cover. They are not abundant, are concentrated in Ass/Bss, and are in general small in size; this indicates that they may have been produced by small shrubs, grasses or forbs. Rarely, long rhizohaloes, more than 2 m deep, can be observed, which probably indicate the presence of isolated trees (Fig. 5A and B).

5.3. Genetic difference of the two pedotypes and their palaeoenvironmental significance

In the studied interval of the Esplugafreda Formation, the Pont d'Orrit pedotype occurs until level 22.90 m from the base of the measured section, whereas the overlying portion is characterised by the Areny pedotype (Fig. 2). Despite both pedotypes being identified as Vertisols, they have significant differences that suggest important palaeoenvironmental changes. These differences, which are discussed in more detail below, can be summarised as follows (Table 1): (i) the Areny pedotype exhibits Bssg horizons, which are characterised by a dominant yellow or olive yellow colour. (ii) Goethite (FeO(OH)) prevails in Bssg horizons. (iii) Gypsum, in the form of lumps that appears to be casts of root holes, or filling slickenside fractures, is exclusive of Bssg horizons. (iv) Deep sealed cracks with greyish green depletion margins are observed only in the Areny pedotype. (v) Horizons with calcium carbonate nodules (Bssk) are typical of the Pont d'Orrit pedotype, and are nearly absent in the Areny pedotype. (vi) The Pont d'Orrit pedotype is dominantly reddish brown or red with localised greyish green mottles. (vii) Haematite (Fe₂O₃) is the dominant oxide of the Pont d'Orrit pedotype. (viii) Aggregates of Microcodium are abundant in all the horizons of Pont d'Orrit pedotype, and are instead absent in Bssg horizon, and extremely rare in the other horizons of the Areny pedotype.

Vertisols are characterised by low hydraulic conductivity, which is closely linked to their high clay content. After a rainfall event or a river flood, water penetrates the soil matrix for a few decimetres only, mainly through cracks or root holes. When the cracks and root holes are completely filled, the water can stagnate in and on the soil for many days. After the soil becomes water saturated, rapid oxygen consumption pushes the slacking waters into anoxia, or “aquic conditions” (Vepraskas, 2015), which leads to form redoximorphic features. In palaeosols, aquic conditions can be inferred

by the presence of abundant redoximorphic features, which form by “processes of reduction, translocation and oxidation of Fe and Mn oxides” in periodically saturated soils (Vepraskas, 2015, pag. 5).

Aquic conditions are demonstrated in Bssg horizons of the Areny pedotype by many redoximorphic features (i.e., features occupying >20% of the exposed surface; Vepraskas, 2015), which can be observed in hand rock specimens and in thin section. In hand specimens: (i) redox concentrations correspond to yellow (10YR 7/8) masses of variable shape on the slickenside surfaces or within the soil matrix (or groundmass) (Figs. 11B and 14B); in some cases, the horizon is almost entirely yellow, indicating that the entire matrix shows impregnative Fe/Mn compounds (Fig. 13A); (ii) redox depletions are greyish-green bodies of variable shape within the matrix, on the slickensides surfaces (Fig. 11B) and at the edges around filled bioturbation holes (Fig. 14B) and sealed cracks (Fig. 13A). In thin section: (i) impregnative redox pedofeatures are observed as amiboidal masses within the angular blocky micropeds (Fig. 11C) or inside filled cracks (Fig. 11E), as external hypo-coatings around relicts of calcareous nodules (Fig. 13C) and as small nodules (Fig. 11D); (ii) redox depletion occurs as internal hypo-coating of angular blocky micropeds (Fig. 11C), as Fe-oxide-depleted groundmass and as small greyish-green rhizohaloes (Fig. 11F).

Aquic conditions are also revealed by the Fe oxides and hydroxides distribution. Haematite is the most common Fe oxide of the Esplugafreda Formation (Fig. 9). It is originally contained in the parent material (C horizon) and diffused in Bss, Bssk and Ass/Bss. Yet, haematite does not occur in Bssg horizons, where this is substituted by goethite, a hydroxide. Since goethite is not present in the parent material (C horizon), this mineral is likely to be the product of the alteration of haematite. De facto, this may reflect how, in presence of water, Fe oxides (mainly haematite) are rapidly weathered to hydroxides (goethite) (Okrush and Frimmel, 2020), which leads to a change in soil colour from reddish brown to yellow or olive yellow (PiPujol and Buurman, 1994; Vepraskas, 2015).

Other evidence of the higher palaeomoisture content of the Areny pedotype is indicated by (i) the scarcity or absence within the profiles of pedogenic calcium carbonate nodules (viz. Bssk horizons) and (ii) the presence of deep sealed cracks. (i) In the development of the Areny pedotype, during the wet season the moisture was high enough to cause leaching of dissolved calcium carbonate from the soil profile; this contrasts with the conditions of development of the Pont d'Orrit pedotype, where lower humidity and high potential evapotranspiration brought about CaCO₃ precipitation in subsurface Bssk soil horizons (Zamanian et al., 2016). (ii) In Vertisols the depth of the cracks is proportional to the soil humidity (Ahmad, 1983; Elias et al., 2001b); therefore the deeper cracks of the Areny pedotype indicate higher and deeper-reaching humidity during the development of this palaeosol, compared to the Pont d'Orrit pedotype.

The Pont d'Orrit pedotype is characterised by an extensive reddish brown colour. Redox depletions circumscribe rhizohaloes and small bodies (mottles) on the slickensides surfaces, mainly concentrated in Ass/Bss horizons; redox concentrations are limited to few Fe/Mn oxides coatings or hypo-coatings and nodules. Thus, it can be deduced that the Pont d'Orrit pedotype developed under local and temporary aquic conditions in stagnant water, probably after short-duration rainfall events.

Aquic conditions can develop due to water saturation of the lower portion of the soil driven by ground water (endosaturation), or due to saturation of the upper portion of the soil by superficial water (episaturation) (Vepraskas, 2015). Since the tops and bottoms of the palaeosols profiles in the

Esplugafreda Formation cannot be readily identified due to the cumulative character of these palaeosols, it is not straightforward to determine whether the redoximorphic features are forms of ground-water gley by endosaturation or of surface-water gley (pseudogley) by episaturation (PiPujol and Buurman, 1998). However, it is possible to infer that the aquic conditions of the Areny pedotype are a consequence of surface-water gleying, in relation to a perched water table that brought about reduction, translocation and oxidation of the Fe. In the Areny pedotype, redox depletion features developed in fractures (slickensides or deep cracks), root holes (rhizhaloes), bioturbations and rims of the micropeds (internal hypo-coating of angular blocky micropeds); this indicates that reducing conditions due to water stagnation developed exclusively in macropores. Therefore, in the Areny pedotype the water did not saturate the entire matrix of the soil, as in ground-water gleying, as the rest of the soil matrix held air inside the pores and was in oxidising conditions. Redox depletion features (depletion in root holes - rhizhaloes - and on the surface of the slickensides), are also present in the Pont d'Orrit pedotype, indicating that even in this case reducing conditions only existed in macropores of the upper horizons (Ass/Bss and Bss) but absent in the lower horizons (Bssk); this testifies to a rate of saturation and reduction lower than that observed in the Areny pedotype and limited to the upper part of the palaeosol profile.

Another deduction can be made based on the identification of these pedotypes as Vertisols. Modern Vertisols are easily subjected to surface-water gleying because they possess high-density parent material and low hydraulic conductivity. In semi-arid climates, such as the climatic conditions that may have been dominant during the time of deposition of the Esplugafreda Formation (Dreyer, 1993; Pujalte et al., 2014), the water can remain stagnant on the surface and in the upper part of the soil for many days and weeks after major rainfall episodes. For instance, in modern soils and ancient palaeosols, various authors (Kraus and Aslan, 1993; Driese et al., 1995; Coulombe et al., 1996; Kraus and Hasiotis, 2006; Buol et al., 2011) described conditions of surface-water gleying caused by a perched water table that was established after rainfalls or floods.

Though an unambiguous determination of the cause of the higher moisture related to the Areny pedotype as being from increased precipitation or flooding cannot be made, the second hypothesis is preferred, because river floods would have presumably led to an increase in the frequency of depositional events; this, in turn, would have resulted in a sedimentary succession consisting almost exclusively of non-pedogenised deposits or at least in a significant proportion of compound palaeosol profiles, expressed by a clear alternation of unaltered deposits and palaeosols (Kraus, 1999), which is not observed.

An apparent contradiction with the hypothesis that the Areny pedotype represents wetter climate conditions is the presence of gypsum in Bssg horizon. Gypsum occurs as lumps that developed in root holes and filled some slickensides fractures, but is absent within the groundmass and in the other horizons of the same pedotype. Furthermore, gypsum is completely absent in the Pont d'Orrit pedotype, which does not bear evidence of aquic conditions. Dreyer (1993), Pujalte et al. (2014) and Chen et al. (2018) claimed that gypsum provides evidence of arid climate during deposition of the Esplugafreda Formation. However, although the gypsum in modern soils of arid environments commonly appears as small lenticular poikilitic forms within the micromass (Podwojewski, 1995; Coulombe et al., 1996; Amit and Yaalon, 1996; Kovda and Mermut, 2010; Poch et al., 2010), the gypsum observed in Bssg horizons studied here only fills macropores consisting of root holes and slickensides fractures. The presence of gypsum in the Areny pedotype can be explained by the existence of aquic conditions and by the significant variation of moisture in the soils between the wet and dry season. During the rainy season, the upper portion of the soil was temporarily water-

saturated, promoting reducing conditions. In this anaerobic state, sulphides such as pyrite could have formed from bacterial activity (Coulombe et al., 1996). Subsequently, in seasonally drier and better drained conditions, the pyrite may have undergone oxidation, and may be completely dissolved to Fe^{2+} and SO_4^{2-} , thus producing sulphuric acid (H_2SO_4) and sulphate minerals such as gypsum ($\text{CaSO}_4 \cdot 2\text{H}_2\text{O}$) (van Breemen and Buurman, 2002). Gypsum may have then precipitated in microcrystals by aqueous solutions only in macroporosities, due to the low hydraulic conductivity of the Areny pedotype. Evidence of fluid circulation with Ca^{2+} and SO_4^{2-} is recognised by the non-uniform distribution of the gypsum in Bssg horizons. Where the Bssg horizon shows a bowl structure, the gypsum is preferentially concentrated below the micro-depression and progressively becomes less abundant away from the bowl and towards the major micro-high of the gilgai microtopography (Fig. 12). This demonstrates that fluid circulated from high to low areas of the soil profile, and stagnated below the micro-depressions where gypsum precipitated. Currently these processes occur in coastal Vertisols, where the source of sulphur is seawater, either directly by marine transgression or by the influence of saline groundwater and aerosols (van Breemen and Buurman, 2002). The Esplugafreda Formation was deposited in close proximity to a marine environment. Notably, two transgressive beds of marine deposits are observed near Serraduy (c. 15 km NW of the study section presented in this article) in the upper portion of the Esplugafreda Formation, which approximately corresponds to the stratigraphic position of the Areny pedotype (Pujalte et al., 2014). However, a marine influence does not need to be invoked to justify the origin of the sulphur in these palaeosols. Pester et al. (2012) documented the sulphur cycle in freshwater wetlands (viz. Histosols and some types of Vertisols), free of sulphate input from a marine source or the parent material.

In the Esplugafreda Formation, *Microcodium* appears mainly fragmented as parent material of the palaeosols, and less commonly as aggregates in situ. *Microcodium* aggregates are abundant in all the horizons of the Pont d'Orrit pedotype, instead they are very rare in the Areny pedotype, and notably absent in Bssg horizons. *Microcodium* is believed to be generated by mycelial saprotrophic organisms associated with actinobacteria, which occur in aerated Ca-rich soils (Kabanov et al., 2008). It is probable that the temporarily saturated and anaerobic conditions associated with the development of the Areny pedotype could have generated inhospitable living conditions for these organisms, thereby limiting their presence to aerated horizons.

In conclusion, the uppermost portion of the Esplugafreda Formation consists of two palaeosol types, both characterised by strongly seasonal climate and included in the order Vertisols. However, based on the inferred climatic parameters, the two types of Vertisols can be assigned to two different suborders (Soils Survey Staff, 2017; Buol et al., 2011, its Fig. 12.6). The Areny pedotype shows aquic conditions, probably linked to increased precipitation in comparison with the Pont d'Orrit pedotype. Thus, the palaeosols of Areny pedotype may be classified as Usterts or Uderts, which are soils characterised by a monsoonal climate and seasonal precipitations. The Pont d'Orrit pedotype can be associated with more arid soils, marked by some seasonal precipitations, such as the Mediterranean Vertisols (Xererts) (Fig. 17). This classification is only a tentative, but highlights the key differences between the two pedotypes.

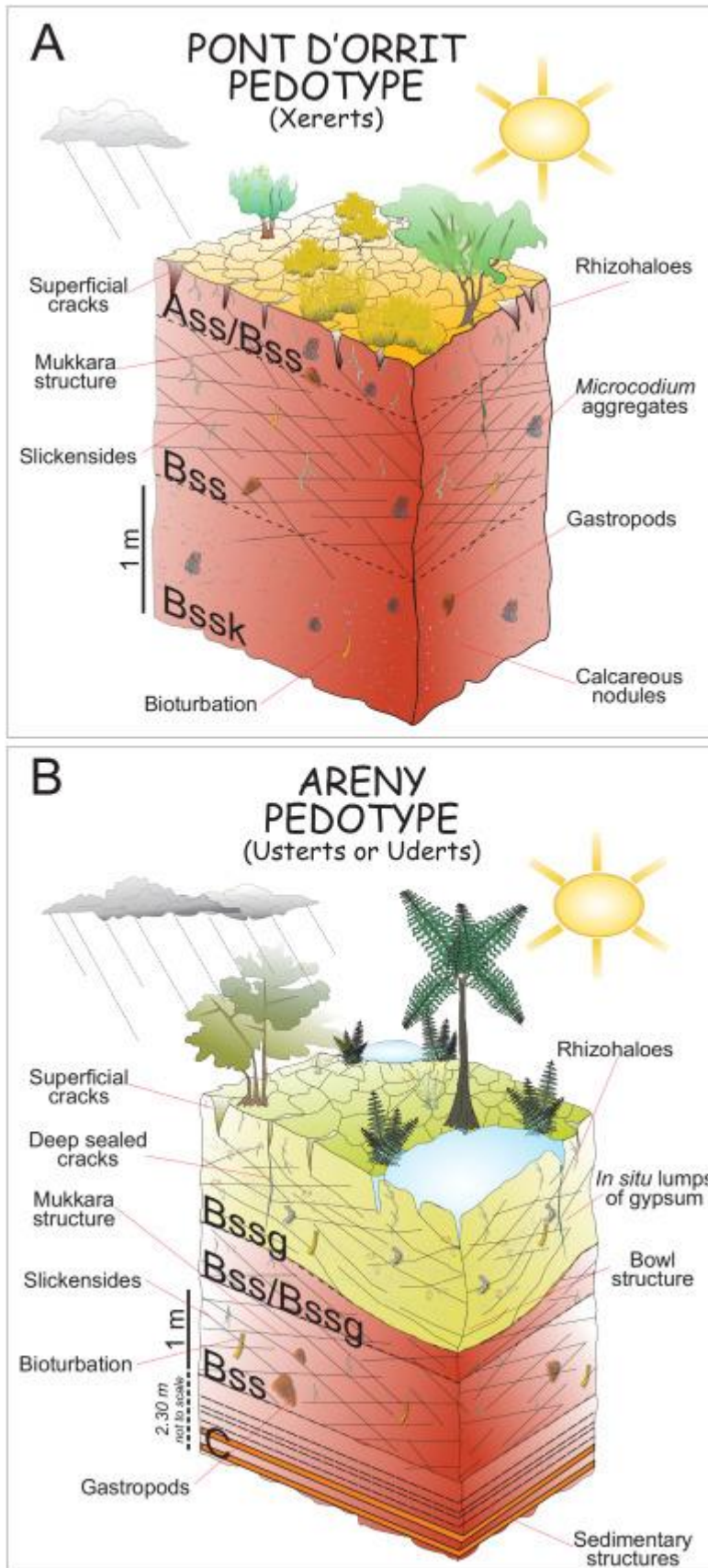


Fig. 17. Cartoon showing the palaeoenvironmental interpretation of the Pont d'Orrit and Areny pedotypes. Note that the representation of the vegetal cover, although compatible with the Paleocene vegetation, is speculative.

5.4. Pedogenic record of climatic variations

Scientific interest in the Tremp Group, to which the studied succession belongs, is in part spurred by the recognition of a stratigraphic record of the PETM, which is identified in the second and third members of the Claret Formation, overlying the Esplugafreda Formation (Fig. 1), where the hyperthermal event is marked by a strong negative $\delta^{13}\text{C}$ excursion (Schmitz and Pujalte, 2003, Schmitz and Pujalte, 2007; Domingo et al., 2009; Manners et al., 2013). The studied section lies below the Paleocene-Eocene boundary, and can therefore provide insight into the prevalent climatic conditions prior to the PETM. In this work, we have demonstrated that the upper portion of the Esplugafreda Formation records a climatic change interpretable as associated with an increase in precipitation, whereby Vertisols developed under a semi-arid climate (Xererts) transitioning vertically to wetter Vertisols (Usterts or Uderts) bearing evidence of aquic conditions. Thus, this study reveals a climatic control on palaeosol characteristics that was previously deemed as likely unimportant for this succession (Dreyer, 1993).

A detailed understanding of the timing and timescale of the climatic variations expressed in the palaeosols, and of whether they could represent a local signal within a global trend, is hampered by the lack of chronometric constraints, and by the general coarseness of the existing chronostratigraphic framework. The studied section spans a stratigraphic interval that only records reverse magnetic polarities, but whether this interval is limited to the magnetozones C24r is not clear, as it may encompass C25r (López-Martínez et al., 2006). Furthermore, the studied late Paleocene record is associated with important stratigraphic discontinuities, both locally, because the measured section underlies a palaeovalley fill (member 1 of the Claret Formation), as well as more broadly across the study area, because interfluvial surfaces acted as morphological highs between the palaeovalleys were themselves partly eroded at the Paleocene-Eocene boundary (Pujalte et al., 2014; Colombera et al., 2017). The temporal magnitude of the gap between the Esplugafreda and the Claret formations is not known. Although this gap can be inferred to have been relatively short given the relatively steady generation of accommodation space that characterised the sedimentary basin at the time (Fernández et al., 2012), the presence of an erosional surface with significant relief between the Esplugafreda and the Claret formations impedes extrapolation of the inferred aggradation rate of the floodplains of the Esplugafreda alluvial system. Yet, the aggradation rate estimated herein (c. 0.5 m/kyr) is of similar magnitude to speculative estimates made by Pujalte et al. (2014) for member 1 of the Claret Formation. If our quantification is taken as an upper-end estimation of the aggradation rate for the study section, the time gap between the top of the studied section and the CIE would be ca. 110 kyr. However, the true rate, averaged over the entire interval, is likely to be smaller, given the expected dependency of aggradation rates on the time over which they are computed (i.e., because the duration of breaks in sedimentation tend to increase on average as the length of time in the stratigraphic section increases, cf. Sadler, 1981). Thus, the time gap between the studied section and the PETM may well be larger than estimated. Nevertheless, based on a similar consideration, the timespan represented by the measured section can be inferred to have been at least c. 180 kyr.

The studied section falls within a stratigraphic interval that should embody the long-term late Paleocene warming trend (Kennett and Stott, 1991a, Kennett and Stott, 1991b; Zachos et al., 2001), which may have been driven by a release of mantle-derived CO_2 associated with magmatism in the North Atlantic igneous province (Thomas and Bralower, 2005). It is significant that the considered section is part of a broader stratigraphic interval that appears to record a trend towards more perennial river discharge and wetter climatic conditions, testified by facies change in the channel

deposits of member 1 of the Claret Formation and by palaeosol colours in associated overbank deposits (Dawson et al., 2014; Colombera et al., 2017); this trend ultimately culminated in the PETM. In this perspective, the documented palaeosol variations may represent a partial record of a progressive strengthening of the hydrologic cycle through the late Paleocene warming trend (cf. Bice and Marotzke, 2002; Kender et al., 2012).

6. Conclusions

This paper considers the palaeopedogenised alluvial deposits of the Esplugafreda Formation, which constitute more than 80% of the entire thickness of the studied succession.

Within the uppermost portion of this unit two pedotypes are recognised: the Pont d'Orrit, and the Areny pedotypes. These pedotypes are identified as Vertisols on the basis of: (i) high content of montmorillonite, (ii) slickensides separating wedge-shape and angular blocky peds and forming mukkar structures, (iii) bowl structures, and (iv) micromorphological porphyric c/f related distribution patterns. The intensity of the slickensides demonstrates that both palaeosol types formed in a climate characterised by strong seasonal moisture variations. Diffuse distinctness of horizon boundaries and large thickness of the palaeosol profiles permit the recognition of these palaeosols as cumulative.

Although these pedotypes belong to the same order, they have significant differences that allow discrimination of two distinct palaeoenvironments. The Pont d'Orrit, which is dominant in the lower portion of the Esplugafreda Formation, has (i) a reddish brown homogenous colour, (ii) diffuse haematite oxides, (iii) few (<20% on the exposed surface) redoximorphic features mostly concentrated in the upper Ass/Bss horizon, and (iv) widespread pedogenic calcareous nodules in lower Bssk horizons. Semi-arid climate conditions with marked seasonal variations can be attributed to these palaeosols. The Areny pedotype, which is dominant in the upper portion of the section, consists of (i) a yellow upper Bssg horizon, which shows abundant (> 20% on the exposed surfaces) redoximorphic features and goethite hydroxides minerals, (ii) a lower reddish brown Bss horizon, (iii) gypsum in macropores, and (iv) scarcity or absence of calcareous pedogenic nodules. This pedotype records formation in more humid (aquic) conditions. Gypsum is not attributed to aridity, but rather to the possible dissolution of pyrite, formed by bacterial activity in aquic conditions, to Fe²⁺ and SO₄²⁻; the resulting sulphuric acid (H₂SO₄) having combined with Ca during the drier season, leading to gypsum precipitation in macropores. Types and distribution of the redoximorphic features indicate that the moisture of the Areny pedotype is tied to surface-water gleying (pseudogleying). Thus, an increase in moisture of the Areny pedotype seems to be associated with surface water, probably an increase in precipitation rather from floods. In fact, flooding would have produced an increase in sedimentation leading to the replacement of cumulative palaeosols by compound palaeosols or unweathered deposits, which are not significant in the uppermost portion of the study section.

The transition from the Pont d'Orrit to Areny pedotypes represents an increase in palaeoprecipitation, occurring in a palaeoclimate context characterised by strong seasonal distribution of humidity. This climatic variation falls within the steady warming trend that heralded the strong increase in temperature at the Paleocene-Eocene boundary, the PETM, which at this palaeolatitude likely caused an intensification of precipitation. The nature of palaeoenvironmental change prior to and through the PETM in this area can be further elucidated by expanding the analyses undertaken herein to the overlying stratigraphy.

Acknowledgements

We are grateful to the two reviewers (Karol Jewula and TSW) for their accurate review and to the Editor-in-Chief and Associate Editor for their editorial endorsement. This research was supported by Conselho Nacional de Desenvolvimento Científico e Tecnológico (CNPq) of Brazil, n. 428531/2018-0 and by Fundação de Amparo à Pesquisa do Estado de São Paulo (FAPESP), n. 2018/10574-8. Josué Davi de Paula, Eufrásio José de Carvalho and Dr. Dailto Silva (State University of Campinas, Brazil) are acknowledged for technical help.

References

- Ahmad, N., 1983. Vertisols. In: Wilding, N L.P., Smeck, E., Hall, G.F. (Eds.), *Pedogenesis and soil taxonomy II. The soil orders. Developments in Soil Science 11B*. Elsevier, Amsterdam, pp. 91-123.
- Ahmad, N., Mermut, A. (Eds.), 1996. *Vertisols and Technologies for their Management. Developments in Soil Science, 24*. Elsevier, Amsterdam, pp. 549.
- Allen, P.A., Allen, J.R., 2005. *Basin analysis. Principles and applications*. Blackwell Publishing, pp.549.
- Amit, R., Yaalon, D.H., 1996. The micromorphology of gypsum and halite in reg soils - the Negev desert, Israel. *Earth Surface Processes and Landforms, 21*, 1127-1143.
- Andrews, E., White, T. del Papa, C., 2017. Paleosol-based paleoclimate reconstruction of the Paleocene-Eocene Thermal Maximum, northern Argentina. *Palaeogeography, Palaeoclimatology, Palaeoecology, 471*, 181–195.
- Arévalo, O.J., Colombera, L., Mountney, N.P., Basilici, G., Marcus Soares, M.V.T, 2022. Variations in water discharge at different temporal scales in a mud-prone alluvial succession: the Paleocene-Eocene of the Tremp-Graus Basin, Spain. 106122, doi.org/10.1016/j.sedgeo.2022.106122.
- Asadzadeh, S., Souza Filho, C.R., 2016. A review on spectral processing methods for geological remote sensing. *International Journal of Applied Earth Observation and Geoinformation, 47*, 69–90.
- Baceta, J.I., Pujalte, V., Wright, V.P., Schmitz, B., 2011. Carbonate platform models, sea level changes and extreme climatic events during the Paleocene/early Eocene greenhouse interval. In: Arenas, C., Pomar, L., Colombo, F. (Eds.), *Pre-meeting Fieldtrips Guidebook, 28th IAS Meeting, Zaragoza Sociedad Geológica de España, Geo- Guías. 7*. pp. 101–150.
- Basilici, G., 2000. Floodplain Lake Deposits on the Early Pleistocene Alluvial Plain (Tiberino Basin, Central Italy). In: Gierlowki-Kordesh, Kelts, K.R., (Eds.) *Lake Basin through space and time. AAPG Studies in Geology, 46*, 535-542
- Basilici, G., Dal' Bo, P. F. F., 2010. Anatomy and controlling factors of a Late Cretaceous Aeolian sand sheet: The Marília and the Adamantina formations, NW Bauru Basin, Brazil. *Sedimentary Geology, 226*, 71–93.
- Basilici, G., Dal' Bo, P. F., Olivera, E. F., 2016. Distribution of palaeosols and deposits in the temporal evolution of a semiarid fluvial distributary system (Bauru Group, Upper Cretaceous, SE Brazil). *Sedimentary Geology, 341*, 245–264.
- Basilici, G., Hechenleitner, E.M., Fiorelli, L.E., Dal' Bo, P.F., Mountney, N.P., 2017. Preservation of titanosaur egg clutches in Upper Cretaceous cumulative palaeosols (Los Llanos Formation, La Rioja, Argentina). *Palaeogeography, Palaeoclimatology, Palaeoecology, 482*, 83–102.
- Bice, K. L., & Marotzke, J. (2002). Could changing ocean circulation have destabilized methane hydrate at the Paleocene/Eocene boundary?. *Paleoceanography, 17*(2), 8-1.
- Bown, T.M., Kraus, M.J., 1987, Integration of channel and floodplain suites, I. Developmental sequence and lateral relations of alluvial paleosols: *Journal of Sedimentary Petrology, 57*, 587--601.
- Bullock, P., Fedoroff, N., Jongerius, A., Stoops, G., Tursina, T., 1985. *Handbook for Soil Thin Section Description*. Waine Research Publications, Wolverhampton, pp.152.
- Buol, S.W., Southard, R.J., Graham, R.C., McDaniel, O.A., 2011. *Soil Genesis and Classification*. Sixth edition. Wiley-Blackwell, Oxford, p. 543.

- Carmichael, J.M., Inglis, G.N., Badger, M.P.S., Naafs, B.D.A., Behrooz, L., Rimmelzwaal, S. Monteiro, F.M., Rohrsen, M., Farnsworth, S., Buss, H.L., Dickson, A.J., Valdes, P.L. Lunt, D.J., Pancost, R.D., 2017. Hydrological and associated biogeochemical consequences of rapid global warming during the Paleocene-Eocene Thermal Maximum. *Global and Planetary Change*, 157, 114-138
- Catt, J.A., 1990. Paleopedology manual. *Quaternary International*, 6, 1–95.
- Charles, A.J., Condon, D.J., Harding, I.C., Palike, H., Marshall, J.E.A., Cui, Y., Kump, L., Croudace, I.W., 2011. Constraints on the numerical age of the Paleocene– Eocene boundary. *Geochemistry Geophysics Geosystems*. 12, Q0AA17.
- Chen, C., Guerit, L., Foreman, B.Z., Hassenruck-Gudipati, H.J., Adatte, T., Honegger, L., Perret, M., Sluijs, A., Castelltort, S., 2018. Estimating regional flood discharge during Palaeocene-Eocene global warming. *Scientific Reports, Nature*, 13391, 1-8.
- Clark, R.N., 1999. Spectroscopy of rocks and minerals and principles of spectroscopy. In: Rencz, A.N. (Ed.), *Remote Sensing for the Earth Sciences: manual of remote sensing*, third ed., 3. John Wiley and Sons, New York, pp. 3–58
- Colombera, L., Arévalo, O.J., Mountney, N.P., 2017. Fluvial-system response to climate change: The Paleocene-Eocene Trepmp Group, Pyrenees, Spain. *Global and Planetary Change* 157, 1–17.
- Coulombe, C.E., Wilding, L.P., Dixon, J.B., 1996. Overview of Vertisols: characteristics and impacts on society. *Advances in Agronomy*, Elsevier, 57, 289-375.
- Cuevas, J.L., 1992. Estratigrafía del “Garumniense” de la Conca de Trepmp. *Prepirineo de Lérida. Acta Geol. Hisp.* 27, 95–108 (in Spanish).
- Daniels, J.M., 2003. Floodplain aggradation and pedogenesis in a semiarid environment. *Geomorphology* 56, 225–242.
- Dawson, A., Grimes, S., Ellis, M., Duller, D., Watkinson, M., Stokes, M., Leng, M.J., 2014. Initial paleohydrological observations from the Paleocene-Eocene boundary at Esplugafreda and Berganuy in northern Spain. *Rend. Online Soc. Geol. It.*, 31, 54-55
- Domingo, L., López-Martínez, N., Leng, M. J., & Grimes, S. T. (2009). The Paleocene–Eocene Thermal Maximum record in the organic matter of the Claret and Tendrúy continental sections (South-central Pyrenees, Lleida, Spain). *Earth and Planetary Science Letters*, 281(3-4), 226-237.
- Dreyer, T., 1993. Quantified fluvial architecture in ephemeral stream deposits of the Esplugafreda Formation (Paleocene), Trepmp-Graus Basin, northern Spain. In: Marzo, M., Puigdefábregas, C. (Eds.), *Alluvial sedimentation: International Association of Sedimentologists Special Publication*. 17. pp. 337–362.
- Driese, S.G., Simpson, E.L., Eriksson, K.A., 1995. Redoximorphic paleosols in alluvial and lacustrine deposits, 1.8 GA Lochness Formation, Mount Isa, Australia: pedogenic processes and implications for paleoclimate. *Journal of Sedimentary Research*, A65, 675-689.
- Duchaufour, P., *Pedogenesis and classification*. George Allen & Unwin, London, pp. 448.
- Dudal, R., 1963. Dark clay soils of tropical and subtropical regions. *Soil Science* 95, 264-270.
- Dudek, M., Waroszewski, J., Kabala, C., Labaz, B., 2019. Vertisols properties and classification in relation to parent material differentiation near Strzelin (SW Poland). *Soil Science Annual*, 70, 158–169.
- Elias, E.A., Salih, A.A., Alaily, F., 2001b. Cracking patterns in the Vertisols of the Sudan Gezira at the end of dry season. *Int. Agrophysics*, 15, 151-155.
- Elias, E.A., Salih, F.M., Salih, A.A., Alaily, F., 2001a. Selected morphological characteristics of soils from Gezira Vertisols, with particular reference to cracking. *Int. Agrophysics*, 15, 79-86.
- Eswaran, H. and Cook, T., 1988. Classification and management-related properties of Vertisols. In: Jutzi, S.C., Haque, I., McIntire, J., Stares, J.E.S. (Eds), *Management of Vertisols in Sub-Saharan Africa*. ILCA, Addis Ababa, Ethiopia, pp. 64-84.
- Fernández, O., Muñoz, J. A., Arbués, P., & Falivene, O. (2012). 3D structure and evolution of an oblique system of relaying folds: the Ainsa basin (Spanish Pyrenees). *Journal of the Geological Society*, 169(5), 545-559.
- Gastaldo, R.A., Kus, K., Tabor, N., Neveling, J., 2020. Calcic vertisols in the Upper Daptocephalus assemblage zone, Balfour Formation, Karoo Basin, South Africa: implications for Late Permian climate. *Journal of Sedimentary Research*, 2020, 90, 609–628.
- Gile, L.H., Peterson, F.F., Grossman, R.B., 1966. Morphological and genetic sequences of carbonate accumulation in desert soils. *Soil Science*, 101, 347–360.

- Gual i Ortí, V., Forner i Valls, F., 2013. Sobre Vidaliella gerundensis (Vidal, 1883) del Paleogen de Vallibona (els Ports). *Nemus*, 3, 81-92.
- Institut Geològic de Catalunya, 2010. Mapa Geològic de Catalunya: Espills 251-2-2 (64-22), 1:25000
- Jenny, H.J., 1941. *Factors of Soil Formation A system of quantitative pedology*. Dover Publications, New York, pp. 281.
- Joeckel, R.M., Ludvigson, G.A., Kirklande, J.I., 2017. Lower Cretaceous paleo-Vertisols and sedimentary interrelationships in stacked alluvial sequences, Utah, USA. *Sedimentary Geology*, 361, 1–24
- Kabanov, P., Anadón, P., Krumbein, W.E., 2008 - Microcodium: An extensive review and a proposed non-rhizogenic biologically induced origin for its formation. *Sedimentary Geology*, 205, 79–99.
- Kender, S., Stephenson, M.H., Riding, J.B., Leng, M.J., Knox, R.W.O.B., Peck, V.L., Kendrick, C.P., Ellis, M.A., Vane, C.H., Jamieson, R., 2012. Marine and terrestrial environmental changes in NW Europe preceding carbon release at the Paleocene-Eocene transition. *Earth and Planetary Science Letters*, 353–354, 108–120.
- Kennett, J. P., & Stott, L. D. (1991). Abrupt deep-sea warming, palaeoceanographic changes and benthic extinctions at the end of the Palaeocene. *Nature*, 353(6341), 225-229.
- Kennett, J.P., Stott, L.D., 1991. Abrupt deep-sea warming, paleoceneanographic changes and benthic extinctions at the end of the Paleocene. *Nature* 353, 225–229.
- Kovda, I., Mermut, A.R., 2010. Vertic Features. In: Stoops, G., Marcelino, V., Mees, F. (eds.) *Interpretation of Micromorphological Features of Soils and Regoliths*. Elsevier, Amsterdam, pp.109-127.
- Kraus, M. J., Woody, D.T., Smith, J.J., Dukic, V., 2015. Alluvial response to the Paleocene–Eocene Thermal Maximum climatic event, Polecat Bench, Wyoming (U.S.A.). *Palaeogeography, Palaeoclimatology, Palaeoecology*, 435, 177–192.
- Kraus, M.J., 1999. Palaeosols in clastic sedimentary rocks: their geologic applications. *Earth Sci. Rev.* 47, 41–70.
- Kraus, M.J., Aslan, A., 1993. Eocene hydromorphic paleosols: significance for interpreting ancient floodplain processes. *Journal of Sedimentary Petrology*, 63, 453-463
- Kraus, M.J., Hasiotis, S.T., 2006. Significance of different modes of rhizolith preservation to interpreting Palaeoenvironmental and palaeohydrologic settings: examples from Palaeogene palaeosols, Bighorn Basin, Wyoming, U.S.A. *J. Sediment. Res.* 76, 633–646.
- Lindbo, D.L., Stolt, M.H., Vepraskas, M.J., 2010. Redoximorphic Features. In: Stoops, G., Marcelino, V., Mees, F. (eds.) *Interpretation of Micromorphological Features of Soils and Regoliths*. Elsevier, Amsterdam, pp.129-147.
- López-Martínez, N., Dinarès-Turrell, J., & Elez-Villar, J. (2006). Chronostratigraphy of the continental paleocene series from the South Central Pyrenees (Spain): New magnetostratigraphic constraints. *Proceeding of the Climate and Biota of the Early Paleocene*.
- Lucas, G., Montenat, C., 1967. Observations sur les structures internes et le développement des Microcodium. *Bulletin Société Géologique de France*, 7, 909-918
- Lynn, W., Williams, D., 1992. The Making of a Vertisol. *Soil Survey Horizons*, 33, 45-50.
- Machette, N.M., 1985. Calcic soils of the southwestern United States. In: Weide, D.L. (Ed.), *Soils and Quaternary Geology of the Southwestern United States*, *Geol. Soc. Am. Spec. Pap.*, 203, 10–21.
- Mack, G.H., James, W.C., Monger, H.C., 1993. Classification of paleosols. *Geological Society of America Bulletin*, 105, 129-136.
- Manners, H. R., Grimes, S. T., Sutton, P. A., Domingo, L., Leng, M. J., Twitchett, R. J., ... & Lopez-Martinez, N. (2013). Magnitude and profile of organic carbon isotope records from the Paleocene–Eocene Thermal Maximum: Evidence from northern Spain. *Earth and Planetary Science Letters*, 376, 220-230.
- Marriott, S.B., Wright, V.P., 1993. Palaeosols as indicators of geomorphic stability in two Old Red Sandstone alluvial suites, South Wales. *Journal of the Geological Society, London*, 150, 1109-1120.
- McCarthy, P.J. Martini, P., Leckie, D.A., 1997. Anatomy and evolution of a Lower Cretaceous alluvial plain: sedimentology and palaeosols in the upper Blairmore Group, south-western Alberta, Canada. *Sedimentology*, 44, 197-220.
- McCarthy, P.J., Plint, A.G., 2017. A pedostratigraphic approach to nonmarine sequence stratigraphy: a three-dimensional paleosol-landscape model from the Cretaceous (Cenomanian) Dunvegan Formation, Alberta and British Columbia, Canada. In: Driese, S.G., Nordt, L.C. (Eds.), *New Frontiers in Paleopedology and Terrestrial Paleoclimatology: Paleosols and Soil Surface Analog Systems*. SEPM Special Publication, 104, pp. 159-177.

- McGarry, D., 1996. The structure and grain size distribution of Vertisols. In: Ahmad, N., Mermut, A. (Eds.) *Vertisols and Technologies for their Management*. Elsevier Science Developments in Soil, 24, pp. 231-259
- McInerney, F.A., Wing, S.L., 2011. The Paleocene-Eocene thermal maximum: a perturbation of carbon cycle, climate, and biosphere with implications for the future. *Annu. Rev. Earth Planet. Sci.* 39, 489–516.
- Mermut, A.R., Dasog, G.S., Dowuona, G.N., 1996b. Soil morphology. In: Ahmad, N., Mermut, A. (eds.), *Vertisols and Technologies for their Management*. Developments in Soil Science, 24. Elsevier, Amsterdam, pp. 43–61.
- Mermut, A.R., Padmanabham, E., Eswaran, H., Dasog, G.S., 1996a. Pedogenesis. In: Ahmad, N., Mermut, A. (eds.), *Vertisols and Technologies for their Management*. Developments in Soil Science, 24. Elsevier, Amsterdam, pp. 43–61.
- Milroy, P., Wright, P., Simms, M.J., 2017. Dryland continental mudstones: Deciphering environmental changes in problematic mudstones from the Upper Triassic (Carnian to Norian) Mercia Mudstone Group, south-west Britain. *Sedimentology*, 1-33.
- Munsell Color, 2013. *Munsell Soil-Color Charts*. Munsell Color, Grand Rapids, MI.
- Okrush, M., Frimmel, H.E., 2020. *Mineralogy. An Introduction to Minerals, Rocks, and Mineral Deposits*. Springer, Berlin, pp.719.
- Pagani, M., Caldeira, K., Archer, D., Zachos, J.C., 2006. An Ancient Carbon Mystery. *Science*, 314, 1556-1557.
- Pester, M., Knorr, K-H., Friedrich, M.W., Wagner, M., Loy, A., 2012. Sulfate-reducing microorganisms in wetlands - fameless actors in carbon cycling and climate change. *Frontier in Microbiology*, 3, 1-19.
- PiPujol, M.D., Buurman, P., 1994. The distinction between ground-water gley and surface-water gley phenomena in Tertiary paleosols of the Ebro basin, NE Spain. *Palaeogeography, Palaeoclimatology, Palaeoecology* 110, 103-113.
- PiPujol, M.D., Buurman, P., 1998. Analyzing ground-water gley and surface-water (pseudogley) effects in paleosols. *Quaternary International*, 51-52, 77-79.
- Poch,, R.M., Artieda, O., Herrero, J., Lebedeva-Verba, M., 2010. Gypsic Features. In: Stoops, G., Marcelino, V., Mees, F. (Eds.) *Interpretation of Micromorphological Features of Soils and Regoliths*. Elsevier, Amsterdam, pp. 195-216.
- Podwojewski, P., 1995. The occurrence and interpretation of carbonate and sulfate minerals in a sequence of Vertisols in New Caledonia. *Geoderma*, 65, 223-248.
- Puig, J.M., Cabello, P., Howell, J., Arbués, P., 2019. Three-dimensional characterisation of sedimentary heterogeneity and its impact on subsurface flow behaviour through the braided-to-meandering fluvial deposits of the Castissent Formation (late Ypresian, Tremp-Graus Basin, Spain). *Marine and Petroleum Geology*, 103, 661–680.
- Puigdefàbregas, C., Muñoz, J.A., Vergés, J., 1992. Thrusting and foreland basin evolution in the southern Pyrenees. In: McClay, K.R. (Ed.), *Thrust Tectonics*. Springer, Netherlands, pp. 247–254.
- Puigdefàbregas, C., Souquet, P., 1986. Tecto-sedimentary cycles and depositional sequences of the Mesozoic and Tertiary from the Pyrenees. *Tectonophysics* 129, 173–203.
- Pujalte, V., Schmitz, B., 2005. Revisión de la estratigrafía del Grupo Tremp (“Garumniense”, Cuenca de Tremp-Graus, Pirineos meridionales). *Geogaceta* 38, 79–82.
- Pujalte, V., Schmitz, B., Baceta, J.I., 2014. Sea-level changes across the Paleocene–Eocene interval in the Spanish Pyrenees, and their possible relationship with North Atlantic magmatism. *Palaeogeography, Palaeoclimatology, Palaeoecology*, 393, 45–60.
- Retallack, G.J., 1994. The environmental factor approach to the interpretation of paleosols. In: Amundson, R., Harden, J., Singer, M. (Eds.), *Factors in Soils Formation: A Fiftieth Anniversary Retrospective*. vol. 33. Soil Science Society of America, pp. 31–64 (Special Publication).
- Retallack, G.J., 2001. *Soils of the Past: An Introduction to Paleopedology*. Second Ed. Blackwell, Oxford, pp. 404.
- Retallack, G.J., 2005. Pedogenic carbonate proxies for amount and seasonality of precipitation in paleosols. *Geology*, 33, 333–336.
- Rush, W. D., Kiehl, J. T., Shields, C. A., Zachos, J. C., 2021. Increased frequency of extreme precipitation events in the North Atlantic during the PETM: Observations and theory. *Palaeogeography, Palaeoclimatology, Palaeoecology*, 568, 110289.

- Sadler, P. M. (1981). Sediment accumulation rates and the completeness of stratigraphic sections. *The Journal of Geology*, 89(5), 569-584.
- Schmitz, B., Pujalte, V., 2003. Sea-level, humidity, and land-erosion records across the initial Eocene thermal maximum from a continental-marine transect in northern Spain. *Geology* 31, 689–692.
- Schmitz, B., Pujalte, V., 2007. Abrupt increase in seasonal extreme precipitation at the Paleocene-Eocene boundary. *Geology* 35, 215–218.
- Schoeneberger, P.J., Wysocki, D.A., Benham, E.C., Soil Survey Staff, 2012. *Field Book for Describing and Sampling Soils, Version 3.0*. Natural Resources Conservation Service, National Soil Survey Center, Lincoln, NE, pp. 9–14.
- Shields, C. A., Kiehl, J. T., Rush, W., Rothstein, M., Snyder, M. A., 2021 . Atmospheric rivers in high-resolution simulations of the Paleocene Eocene Thermal Maximum (PETM). *Palaeogeography, Palaeoclimatology, Palaeoecology*, 567, 110293.
- Sluijs, A., Brinkhuis, H., Schouten, S., Bohaty, S.M., John, C.M., Zachos, J.C., Reichert, G.J., Sinninghe Damsté J.S., Crouch E.M., Dickens, G.R., 2007. Environmental precursors to rapid light carbon injection at the Paleocene/Eocene boundary. *Nature - Letters*, 450, 1218-1221.
- Soares, M.V.T., Basili, G. Lorenzoni, P., Colombero, L., Mountney, N.P., Martinelli, A.G., Mesquita, A.F., Marinho, T.S., Váscónez, R.G.G., Marconato, A., 2020. Landscape and depositional controls on palaeosols of a distributive fluvial system (Upper Cretaceous, Brazil). *Sedimentary Geology* 409, 105774
- Soil Science Division Staff, 2017. *Soil Survey Manual*. United States Department of Agriculture Handbook, 18, pp.603.
- Soil Survey Staff, 1999. *Soil taxonomy. A Basic System of Soil Classification for Making and Interpreting Soil Surveys*. US Department of Agriculture, Natural Resource Conservation Service, Washington, D.C., p. 871.
- Soil Survey Staff. 2014. *Keys to Soil Taxonomy*, 12th ed. USDA-Natural Resources Conservation Service, Washington, DC., pp.360.
- Stoops, G., Marcelino, V., Mees, F., (Eds.), 2010. *Interpretation of Micromorphological Features of Soils and Regoliths*. Elsevier, Amsterdam, pp. 720.
- Stoops, G., 2003. *Guidelines for Analysis and Description of Soil and Regolith Thin Sections*. Soil Science Society of America, Inc. Madison, Wisconsin, USA, pp. 181.
- Thomas, D. J., & Bralower, T. J. (2005). Sedimentary trace element constraints on the role of North Atlantic Igneous Province volcanism in late Paleocene–early Eocene environmental change. *Marine Geology*, 217(3-4), 233-254.
- van Breemen, N., Buurman, P., 2002. *Soil Formation*. Second Edition. Kluwer academic publishers. New York, Boston, Dordrecht, London, Moscow. pp.404
- van Dijk, J., 2019. *Reconstructing Continental Climates using Clumped Isotopes in Pedogenic Siderites*. Published PhD Thesis, ETH Zurich, pp. 226, <https://doi.org/10.3929/ethz-b-000313375>
- van Dijk, J., Fernandez, A., Bernasconi, S. M., Caves Rugenstein, J. K., Passey, S. R., & White, T., 2020. Spatial pattern of super-greenhouse warmth controlled by elevated specific humidity. *Nature Geoscience*, 13, 739-744.
- Vepraskas, M.J., 2015. *Redoximorphic Features for Identifying Aquic Conditions: North Carolina State University, College of Agriculture and Life Sciences*, pp. 30.
- Vergés, J., Burbank, D.W., 1996. Eocene-Oligocene thrusting and basin configuration in the eastern and central Pyrenees (Spain). In: Friend, P.F., Dabrio, C.R. (Eds.), *Tertiary Basins of Spain: The Stratigraphic Record of Crustal Kinematics*. Cambridge University Press, Cambridge, pp. 120–133.
- Vergés, J., Millán, H., Roca, E., Muñoz, J.A., Marzo, M., Cirés, J., den Bezemer, T., Zoetemeijer, R., Cloetingh, S., 1995. Eastern Pyrenees and related foreland basins: pre-, syn- and post-collisional crustal-scale cross-sections. *Marine and Petroleum Geology*, 12 (8), 903–915.
- Vidal, L. M. 1883. *Edad de las capas de Bulimus gerundensis*. *Memorias de la Real Academia de Ciencias Naturales y Artes de Barcelona 2ª Época*, 1, 343-359.
- Wentworth, C. K., 1922, A scale of grade and class terms for clastic sediments: *Jour. Geology*, 30, p. 377-392.
- Whitchurch, A.L., Carter, A., Sinclair, H.D., Duller, R.A., Whittaker, A.C., Allen, P.A., 2011. Sediment routing system evolution within a diachronously uplifting orogen: insights from detrital zircon thermochronological analyses from the South-Central Pyrenees. *American Journal of Sciences*, 311, 442–482.

- Yaalon, D. H., Kalmar, D., 1978. Dynamics of cracking and swelling clay soils: displacement of skeletal grains, optimum depth of slickensides, and rate of intra-pedonic turbation. *Earth Surface Processes*, 3, 31-42.
- Yong, R.N. and Warkentin, B.P., 1966. *Introduction to Soil Behavior*. Macmillan, New York, pp. 451.
- Zachos, J., Pagani, M., Sloan, L., Thomas, E., & Billups, K. (2001). Trends, rhythms, and aberrations in global climate 65 Ma to present. *science*, 292(5517), 686-693.
- Zachos, J.C., Schouten, S., Bohaty, S., Quattlebaum, T., Sluijs, A., Brinkhuis, H., Gibbs, S.J., Bralower, T.J., 2006. Extreme warming of mid-latitude coastal ocean during the Paleocene-Eocene Thermal Maximum: inferences from TEX86 and isotope data. *Geology* 34, 737–740.
- Zamanian, K., Pustovoytov, K., Kuzyakov, Y., 2016. Pedogenic carbonates: Forms and formation processes. *Earth-Science Reviews*, 157, 1–17.